Controlling the structure of spin-coated multilayer ethylcellulose/hydroxypropylcellulose films for drug release

Citation for the original published paper (version of record):
Carmona, P., Poulsen, J., Westergren, J. et al (2023). Controlling the structure of spin-coated multilayer ethylcellulose/hydroxypropylcellulose films
for drug release. International Journal of Pharmaceutics, 644.
http://dx.doi.org/10.1016/j.ijpharm.2023.123350

International Journal of Pharmaceutics 644 (2023) 123350

Contents lists available at ScienceDirect

International Journal of Pharmaceutics

journal homepage: www.elsevier.com/locate/ijpharm

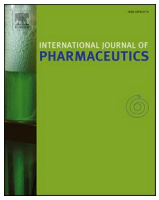

Controlling the structure of spin-coated multilayer ethylcellulose/hydroxypropylcellulose films for drug release

Pierre Carmona [a,b], Jens Poulsen [c], Jan Westergren [c], Torben Nilsson Pingel [a], Magnus Röding [a,d], Eileen Lambrechts [a,e], Herlinde De Keersmaecker [e,f], Kevin Braeckmans [e], Aila Särkkä [d], Christian von Corswant [g], Eva Olsson [b], Niklas Lorén [a,b,*]

[a] Unit Product Design, Department Agriculture and Food, Division Bioeconomy and Health, RISE Research Institute of Sweden, Gothenburg, Sweden
[b] Division Nano-and BioPhysics, Department of Physics, Chalmers University of Technology, Gothenburg, Sweden
[c] Wendelsbergs beräkningskemi AB, Mölnlycke, Sweden
[d] Department of Mathematical Sciences, Chalmers University of Technology and University of Gothenburg, Gothenburg, Sweden
[e] Laboratory of General Biochemistry and Physical Pharmacy, Ghent University, Ghent, Belgium
[f] Ghent Light Microscopy Core, Ghent University, Ghent, Belgium
[g] Oral Product Development, Pharmaceutical Technology & Development, Operations, AstraZeneca, Gothenburg, Sweden

ARTICLE INFO

Keywords:
Cahn-Hilliard simulations
Cellulose
Confocal laser scanning microscope
Electron microscopy
Multilayer film
Phase separation kinetics
Phase separation mechanisms
Porous film for controlled release

ABSTRACT

Porous phase-separated ethylcellulose/hydroxypropylcellulose (EC/HPC) films are used to control drug transport out of pharmaceutical pellets. Water-soluble HPC leaches out and forms a porous structure that controls the drug transport. Industrially, the pellets are coated using a fluidized bed spraying device, and a layered film exhibiting varying porosity and structure after leaching is obtained. A detailed understanding of the formation of the multilayered, phase-separated structure during production is lacking. Here, we have investigated multilayered EC/HPC films produced by sequential spin-coating, which was used to mimic the industrial process. The effects of EC/HPC ratio and spin speed on the multilayer film formation and structure were investigated using advanced microscopy techniques and image analysis. Cahn-Hilliard simulations were performed to analyze the mixing behavior. A gradient with larger structures close to the substrate surface and smaller structures close to the air surface was formed due to coarsening of the layers already coated during successive deposition cycles. The porosity of the multilayer film was found to vary with both EC/HPC ratio and spin speed. Simulation of the mixing behavior and *in situ* characterization of the structure evolution showed that the origin of the discontinuities and multilayer structure can be explained by the non-mixing of the layers.

1. Introduction

In the field of pharmaceutical research, controlled drug release formulations play a pivotal role in delivering medications at predetermined rates and intervals within the body. The primary goal is to minimize undesirable side effects while optimizing the therapeutic efficacy of the drug. One promising approach to drug delivery involves utilizing a pellet that houses a drug reservoir coated with a phase-separated polymer film. Upon contact with bodily fluids, the water-soluble phase of the film dissolves, resulting in the formation of a porous network structure. The structure of the pellet's coating governs the rate at which the drug is released from the core into the surrounding bodily fluids. By meticulously controlling the pellet's manufacturing process and, consequently, the coating structure, it is possible to tailor the drug release rate (Tiwari et al., 2012). Porous polymer phase-separated films have shown good efficiency in controlling drug transport (Marucci et al., 2011). In this work, two cellulose derivatives, water-insoluble ethylcellulose (EC) and water-soluble hydroxypropylcellulose (HPC) are used to make thin phase-separated films. EC and HPC are well-established in the pharmaceutical industry for controlled release applications (Sakellariou and

Abbreviations: 2D, Two dimensions; 3D, Three dimensions; CLSM, Confocal Laser Scanning Microscopy; EC, Ethylcellulose; FIB, Focused Ion Beam; FOV, Field Of View; HPC, Hydroxypropylcellulose; $L(t)$, Characteristic length scale at time t; $m \pm sd$, Mean plus/minus standard deviation; PCT, Percolation to Cluster Transition; SEM, Scanning Electron Microscope; wt%, Weight percentage.

* Corresponding author.
E-mail address: niklas.loren@ri.se (N. Lorén).

https://doi.org/10.1016/j.ijpharm.2023.123350
Received 14 June 2023; Received in revised form 23 August 2023; Accepted 25 August 2023
Available online 26 August 2023

Rowe, 1995). Fig. 1 illustrates the various stages involved in drug release. Upon ingestion of the drug-containing tablet, the phase-separated coating encounters bodily fluids. As a result, the water-soluble HPC dissolves and leaches out, creating a porous network. This porous network serves as a pathway through which the drug can diffuse in a regulated manner. The three-dimensional structure of this porous network ultimately governs the rate of drug transport (Wassén et al., 2014; Gebäck et al., 2015). By controlling the kinetics of the phase separation and the film structure, it is possible to tailor the drug release rate.

In the pharmaceutical industry, the coating of drug-containing pellets with thin phase-separated films is commonly achieved through batch-wise fluidized bed spraying. Specifically, for EC/HPC (ethylcellulose/hydroxypropyl cellulose) coating, the Wurster coating process, a bottom spray fluidized bed technique, is utilized. Within this apparatus, the pellets circulate through the spraying zone and return to the bottom of the device in a continuous loop.

During the process, the polymer mixture is initially in a one-phase state and is sprayed onto the pellets in the spraying zone, forming multiple small droplets that adhere to the core, creating a liquid coating. As the mixture is exposed to the environment, ethanol evaporates, leading to phase separation and an increase in viscosity. Consequently, the film structure becomes kinetically trapped, and a dry coating is formed on the pellet surface. The entire coating sequence involves a series of stages as shown in Fig. 2. Driven by gas circulation (mostly nitrogen), the pellets move from the bed to the spraying zone induced by the spray nozzle. The pellets then return to the bed through chaotic trajectories. Throughout the process, the pellets repeatedly undergo cycles of spraying, wetting, phase separation, and drying until the desired coating thickness is achieved (as shown in Fig. 2).

The structure of such industrial pellets has been analyzed previously using focused ion beam combined with scanning electron microscopy (FIB-SEM), allowing for characterization of the coating microstructure and its porosity, connectivity, and tortuosity (Fager, 2020; Fager et al., 2020a, 2020b, 2021a, 2021b; Röding et al., 2021). According to a recent study by Fager (2020), the EC/HPC coating, after spraying and leaching of the water soluble HPC, is known to have a multilayer structure with layers exhibiting different porosity. These findings have prompted us to hypothesize that the multiple passages cause the layered structure. During each passage through the spraying zone, several droplets are being distributed onto the surface and a thin layer is formed. Each new layer could influence the structure of the already existing layers. Drying of the thin layers induces phase separation and kinetic trapping of the structure between each passage. In addition, the pellets are spinning due

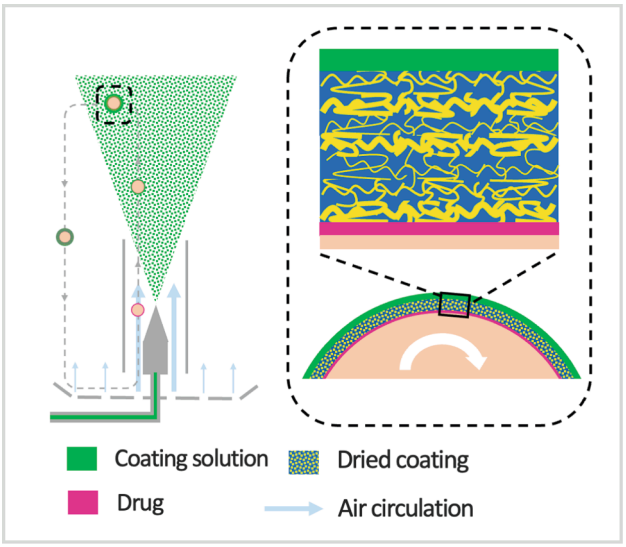

Fig. 2. Schematic illustration of the industrial coating process using a fluidized bed spraying device. On the left, the fluidized bed with the nozzle spraying droplets of coating solution onto the circulating pellets. On the right, the magnified structure of a pellet being coated. Each passage in the spraying zone adds a layer.

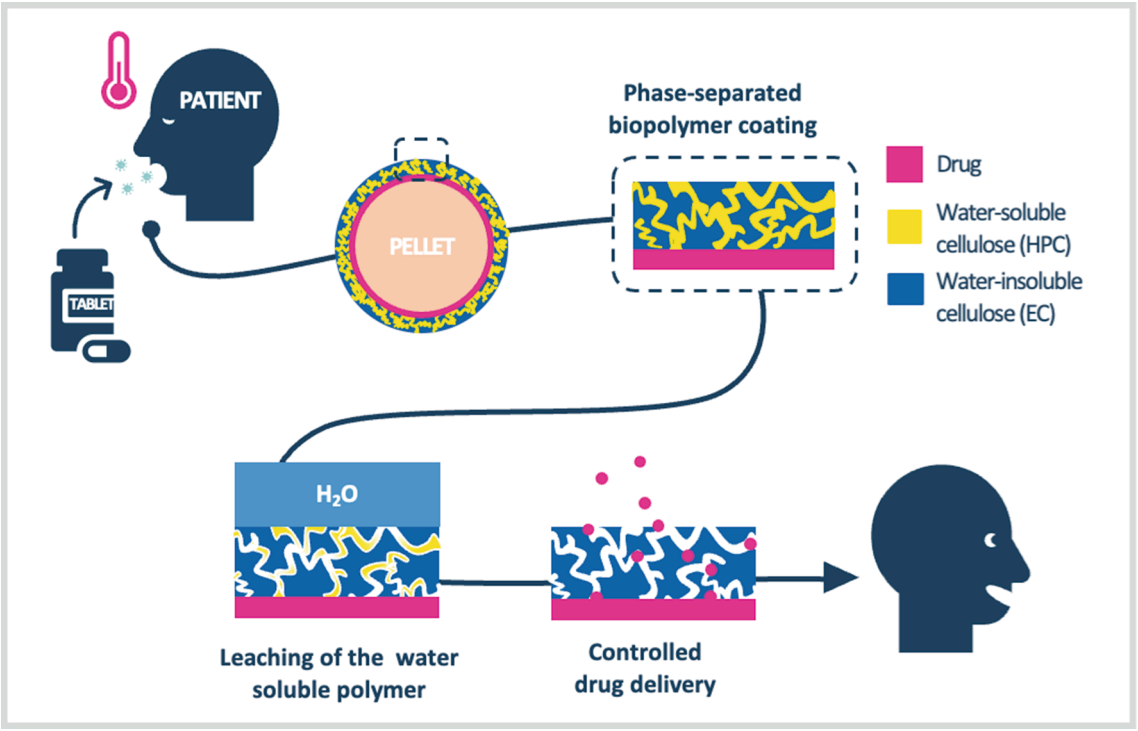

Fig. 1. Schematic illustration of the principle of a drug delivery system with EC/HPC porous films. From top left to bottom right, the patient swallows the tablet consisting of several pellets. The pellets containing the drug are coated with a phase-separated EC/HPC film. When in contact with the body fluids, the water-soluble HPC leaches out, revealing a porous structure through which the drug can be delivered in a controlled manner.

to the gas circulation which can influence the structure formation. In Fig. 2, the formation of a layered structure around a pellet during the coating process is illustrated.

The aims of this work were to understand why the coating structure is layered and why the layers exhibit varying porosity. Nevertheless, the fluidized bed poses significant challenges when attempting to observe structure formation and phase separation during film solvent evaporation. The spray-coating process involves several mechanisms, such as phase separation, kinetic trapping due to viscosity increase, ethanol penetration leading to softening, swelling and coarsening, remixing, and solvent evaporation. In the past, researchers mimicked the Wurster device using a rotating drum and a spray nozzle (Marucci et al., 2011; Fager, 2020; Andersson, 2015). However, it was only possible to investigate the final dried freestanding film structure with this rotating drum technique. A new way to mimic the deposition of a thin layer of EC/HPC using spin-coating, which allows the investigation of the structure evolution *in situ,* has previously been explored (Carmona et al., 2021). Spin-coating entails a method wherein monitoring and understanding phase separation during solvent evaporation in a thin film is significantly more straightforward compared to the industrial process. Spin-coating has been effectively employed to fabricate thin EC/HPC films, and the influence of different spin-coating parameters on the resulting dried structure has been studied (Carmona et al., 2021). It was found that the final characteristic length scale decreases with increasing spin speed. In addition, the film thickness decreases with increasing spin speed and a strong correlation between thickness and spin speed was found for 22 wt% HPC, 30 wt% HPC and 45 wt% HPC which was in accordance with other work in the literature (Meyerhofer, 1978; van Franeker et al., 2015; Williams et al., 2013; Muller-Buschbaum and Stamm, 2001). However, the work by Carmona et al. (2021), was focused on the production of a monolayer through the spin-coating process. In this work, we investigated the production of multilayer films using spin coating, to mimic the structure formation of the multilayer coating around the industrial pellets.

In the literature, one of the most popular methods used to produce multilayered films is the layer-by-layer (LbL) method (Decher, 1997), where multilayer thin films are typically obtained by alternating layers of oppositely charged materials. The LbL approaches are based on sequential adsorption of different materials on a substrate surface driven by different interactions, such as electrostatic interactions, van der Waals forces, and hydrogen bonding. The LbL method has been used, for example, to make spin-coated cellulose xyloglucan multilayered thin films (Cerclier et al., 2010), LbL capsules for drug delivery (Johnston et al., 2006), and spin-coated freestanding films for biomedical applications (Moreira et al., 2021). The formation of layer-by-layer films through spin-coating includes the effect of various parameters such as substrate characteristics, spin speed, spin time, acceleration, and fume exhaust (Chiarelli et al., 2002; Tyona, 2013). In this work, we propose to construct multilayer films by repeated deposition cycles. The layers we produced were made with solutions with the same polymer/ethanol ratio; solely the EC/HPC ratio was varied. In some cases, we used the exact same solution, and varied the spin speed between the layers instead. Using this technique raises the following question: Is it possible to obtain a layered structure using almost identical solutions (only EC/HPC ratio changes or spin speed) to make layers with different porosity and structure?

In previous work (Carmona et al., 2022a, 2022b), the structure evolution during deposition of a monolayer was extensively studied and was used in this work as the basis to understand the structure formation of multilayer films. In these previous studies, the in-plane (Carmona et al., 2022a) and cross-sectional (Carmona et al., 2022b) structure evolution was characterized using confocal laser scanning microscopy (CLSM), profilometry, and image analysis. The effect of the EC/HPC ratio on the structure evolution was investigated. Bicontinuous structures were found for 30 to 40 wt% HPC and discontinuous structures were found for the fractions 15 to 22 and 45 to 85 wt% HPC. The growth of the characteristic length scale followed a power law, $L(t)t^n$, with $n = 1$ for bicontinuous structures, and n = 0.45–0.75 for discontinuous structures. Two main coarsening mechanisms were identified: interfacial tension-driven hydrodynamic growth for bicontinuous structures and diffusion-driven coalescence for discontinuous structures (Carmona et al., 2022a). The characteristic length scale after kinetic trapping ranged between 3.0 and 6.0 μm for bicontinuous structures and between 0.6 and 1.6 μm for discontinuous structures. During the shrinkage of the film, the phase-separated structure underwent a transition from 3D to nearly 2D structure evolution along the surface (Carmona et al., 2022b). The transition was observed when the characteristic length scale of the phase-separated structure closely matched the thickness of the film. Bicontinuous systems exhibited a more pronounced occurrence of this phenomenon. The shrinkage rate remained unaffected by changes in the EC/HPC ratio, while the initial and final film thickness increased with increasing HPC fraction. Additionally, a novel methodology was devised to estimate a segment of the binodal curve within the ternary phase diagram for EC/HPC in ethanol.

During phase separation, the initial quenching process induces the coarsening of the phase-separated structure, causing it to attain a specific domain size. Subsequently, a second quench or a continuation of the first quench can occur, resulting in a secondary phase separation with a smaller length scale compared to the primary phase separation. To visualize this phenomenon, Fig. 3 provides an illustration of the secondary phase separation occurring in a symmetric polymer blend (with a 50/50 volume fraction) during phase separation via spinodal decomposition. Secondary phase separation was observed experimentally in other polymer blends (Tanaka and Araki, 1998; Tanaka, 1994; Kim et al., 1993; Alig et al., 2003; Yamamura et al., 2002), during the spin-coating process (Ebbens et al., 2011; Heriot and Jones, 2005) and was studied through modeling and computer simulations (Henderson and Clarke, 2004; Tran et al., 2006).

As already mentioned, many different mechanisms are involved in the structure formation during the spray-coating process. Here, Cahn-Hilliard simulations of spinodal decomposition and Flory-Huggins (Flory, 1942) theory were used to investigate the mixing behavior during the multilayer film formation (Cahn and Hilliard, 1958; Cahn, 1965). In our system, we needed to simultaneously model the spinodal process in a ternary solvent-polymer–polymer system like described in Huang et al. (1995), as well as the evaporation process. In previous work, simulations where spinodal decomposition and solvent evaporation were handled simultaneously, were performed (Kim et al., 2009; Ronsin et al., 2020; Buxton and Clarke, 2007; Negi et al., 2018; Saylor et al., 2011). The simulations were consistent with the experimental observations in the case of controlled release coatings (Kim et al., 2009; Saylor et al., 2011), thin film mixtures for solar cells (Ronsin et al., 2020), and during film formation by spin-coating (Buxton and Clarke, 2007; Negi et al., 2018). For the simulation of structure evolution in this work, we used the so called “cell model” that was also used in the work from Oono and Puri (1987) and Ren and Hamley (2001).

In this work, spin-coating has been used to mimic the industrial process of fluidized bed spraying. We have characterized the effect of the EC/HPC ratio and spin speed on the film formation process by using CLSM, FIB-SEM, and image analysis. The interactions between a droplet and multilayered films were monitored *in situ*. This paper is structured as follows: (i) controlled production of multilayer films at lab scale using spin-coating, (ii) characterization of the influence of the EC/HPC ratio on the layered structure of multilayer films and the interaction between layers, (iii) determining the influence of spin speed on the multilayer film structure.

2. Material and methods

2.1. Solution preparation

Solutions of HPC (Klucel Pharm HPC, grade LF, Ashland Inc,

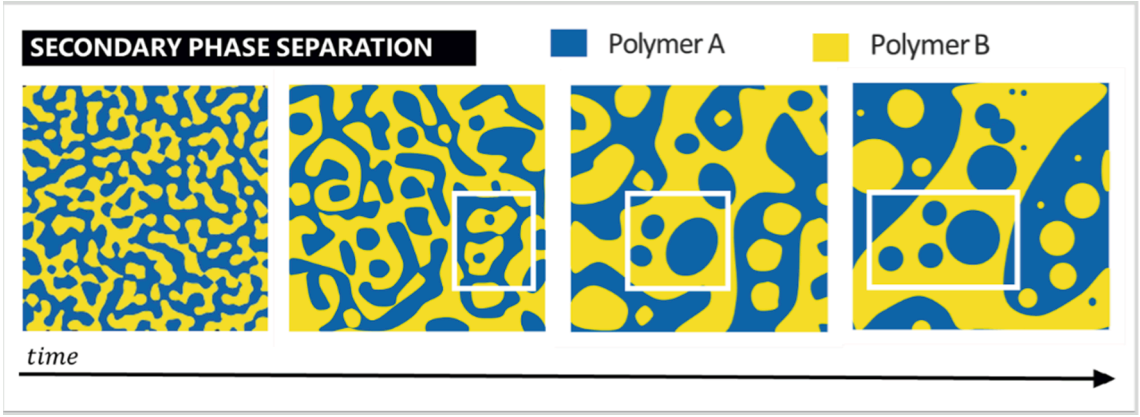

Fig. 3. Schematic illustration of the secondary phase separation during phase separation of a symmetric immiscible polymer blend. During phase separation of polymer A and polymer B, the two phases coarsen and secondary phase separation occurs. The white boxes indicate areas where secondary phase separation is particularly visible. Adapted from Tanaka and Araki (1998).

Covington, Kentucky, USA) with a mean molecular weight of 95 kDa (Ashland, 2017) and EC (Ethocel Standard Premium, viscosity 10 cps, Dow Cellulosics, Dow Chemical Company, Midland, Michigan, USA) with a mean molecular weight of 30 kDa (DowCellulosics, 2005) were prepared. 6 wt% of polymer blends were mixed in a solution of 2 mM Na-fluorescein (CAS. 518-47-8, Sigma Aldrich, St. Louis, Missouri, USA) and ethanol (CAS. 64–17-5 AnalR NORMAPUR® 96 %, VWR Chemical, Radnor, Pennsylvania, USA) and stirred overnight. The EC/HPC polymer ratios studied were 22, 30, 37, 45 and 60 wt% of HPC in the polymer blend.

2.2. Sample preparation by spin-coating

A spin-coater (WS-650MZ-23NPP, Laurell Technologies, North Wales, Pennsylvania, USA) was used to spin-coat the EC/HPC solutions. The volume of the solution was fixed at 200 µL. The polymer solution was deposited on the surface of the substrate: 22 mm diameter round glass bottom petri dishes for the CLSM experiments (HBST-3522, Willco Wells, Amsterdam, Netherlands) and 12.7 mm diameter aluminum pin stub with carbon tape for the SEM and FIB-SEM experiments.

The spin-coater bowl was equipped with a nitrogen flow which ensures a humidity and oxygen free environment. Prior to spin-coating, the solutions were kept in a 25 °C water bath, the substrate was let in the spin coater bowl and the temperature of the spin-coater bowl was 25 ± 1 °C. Fig. 4 shows the production of a multilayer film using spin-coating. The deposition cycle corresponds to the deposition of one layer and is repeated until the desired number of layers is reached. The first step is the deposition of the polymer solution onto the substrate. During this step, the films were first spun at 100 RPM for 25 s, then the polymer solution was deposited and spun at 100 RPM during 5 s (Fig. 4a). The second step corresponds to the film formation with spin speed set at 2000 or 8000 RPM during 1 min with acceleration 2000 RPM/s or 8000 RPM/s (Fig. 4b). The third step is an extra drying step consisting of 4 min spinning at 8000 RPM with acceleration 8000 RPM/s (Fig. 4b to Fig. 4c). The deposition cycle is repeated for additional layers (Fig. 4d). Finally, when the multilayer film is obtained (Fig. 4e), the film is characterized with microscopy and image analysis (Fig. 4f).

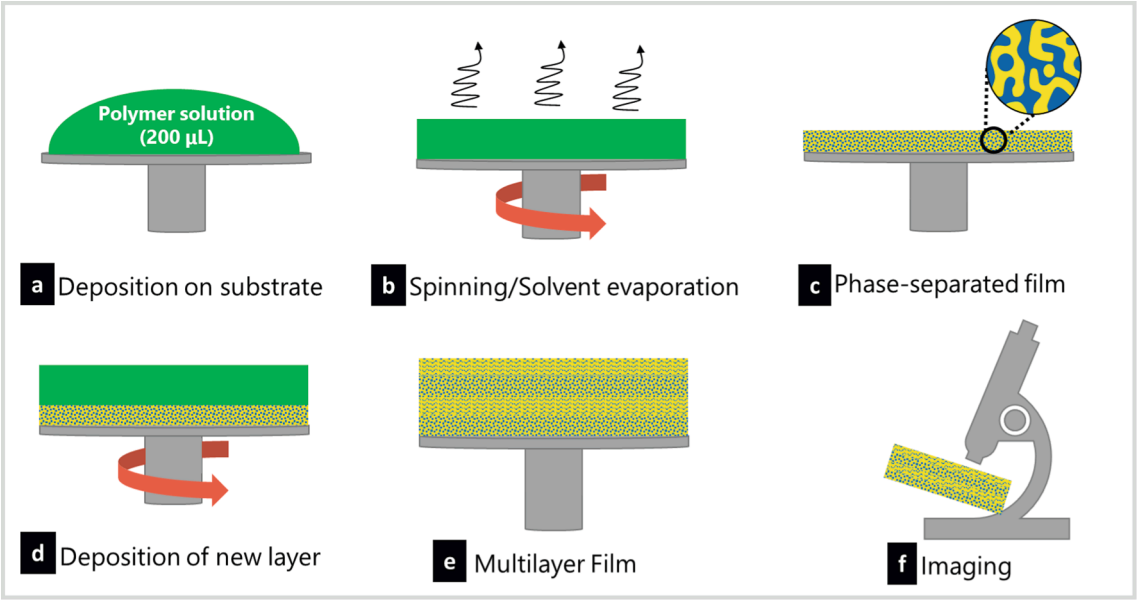

Fig. 4. Schematic illustration of the spin-coating process for production of a multilayer film with a) deposition of the polymer solution (EC and HPC in ethanol) onto the substrate, b) spinning and solvent evaporation inducing phase separation, c) phase-separated film, d) repetition of step a to c to form e) a multilayer film, and f) the film is characterized using microscopy and image analysis techniques.

2.3. Confocal laser scanning microscopy

2.3.1. CLSM for the imaging of multilayer film

The structure of the spin-coated multilayer films was determined using a confocal laser scanning microscope (CLSM; Leica TCS SP5, Leica, Wetzlar, Germany) with a Leica 100x/NA 1.4 PL APO oil objective. A 488 nm argon laser was used for excitation of the Na-fluorescein used to stain the HPC phase. The signal emitted in the interval 500–600 nm was recorded (the fluorescein emission peak is expected at 515 nm). For in-plane measurements, zooms 3x, 3.44x and 8x (FOV 52, 45 and 19 μm respectively) were used, depending on the size of the structure observed. The images were acquired with 1024 × 1024 pixels resolution, a scanning rate of 400 Hz, and a z-step of 0.21 μm between the frames. The latter measurements were performed with a galvanometric stage that can move in the z-direction with high precision, permitting to image a stack of xy-images, producing a xyz-volume. For cross-section measurements a zoom of 3.44x (FOV 45 μm) was used.

2.3.2. In situ CLSM experiment to analyze the structure evolution when a new layer is added to a multilayer film

The structure evolution of the multilayer film after introduction of a droplet onto its surface was determined using a confocal laser scanning microscope (Facility Line, Abberior Instruments, Göttingen, Germany) with an Olympus 60x/NA 1.42/WD 0.15 mm PL APO oil objective (UPLXAPO60XO, Olympus, Tokio, Japan) on an Olympus IX83 inverse microscopy body (motorized). A droplet of 0.1 μL of polymer solution (made as described in 2.1) was deposited onto the surface of a multilayer film (made in 2.2) in the center of the petri dish using a pipette (Transferpette S, 0.1–2.5 μL, Brand, Wertheim, Germany). A 485 nm pulsed diode laser was used for excitation of the fluorescein used to stain the HPC. The signal emitted in the interval 498–608 nm was recorded with the Abberior Spectral Rainbow detection unit (Abberior Instruments, Göttingen, Germany). The pinhole was set to 1 AU. A QUAD scanner was used for unidirectional scanning with a line average of 3 and a pixel dwell time of 1 μs.

After the addition of a droplet, film cross-sections were imaged for 60 min. Images were acquired every 5 s with 1229 × 1200 pixels resolution, with a pixel size of 100 nm. Before the introduction of the droplet and after 60 min (when the film was dried), xyz-stacks of the film were recorded. The images were acquired with 1247 × 1247 pixels resolution, with a pixel size of 100 nm and a z-step of 0.25 μm between frames.

2.4. Scanning electron microcopy

Cross-sectional SEM micrographs of multilayer EC/HPC films were recorded using a scanning electron microscope SEM (JSM-7800F Prime, JEOL, Tokyo, Japan), using the secondary electron detector, at working distance of 10 mm and at 1 kV. The films were spin-coated on carbon tape as described in 2.2. After that, 20 μm cross sections were obtained using a cryostat (CM1900, Leica, Wetzlar, Germany). Leaching was performed as described in Fager (2020) in 1L MilliQ water during 24 h, with gentle agitation. Prior to imaging, and to reduce the charging effects, the cross-section films were coated with 4 nm Au in a sputter coater (EM ACE600 Leica, Wetzlar, Germany).

2.5. FIB-SEM tomography

To obtain a 3D image of EC/HPC multilayer film, FIB-SEM tomography was performed using a Tescan GAIA3 (Tescan, Brno, Czech Republic). Films were made using spin-coating on an aluminum pin stub with carbon tape as described in section 2.2. Leaching was performed as described in Fager (2020) in 1 L MilliQ water during 24 h, with gentle agitation. To reduce charging effects, the film was coated with 20 nm Au in a sputter coater (EM ACE600 Leica, Wetzlar, Germany) and 2 μm Pt was deposited *in situ* with a Gas Injection System (GIS). The method used to realize the FIB-SEM experiment was inspired by Fager et al., 2020a, 2020b; Fager, 2020, 2018). The FIB–SEM tomography software from TESCAN was used to perform the slice-and-image procedure, where the ion beam was used to perform thin slices and the electron beam was used to image the cross-section surface. The angle between the ion and electron beams was 55° and the coincidence point was at a working distance of 5 mm. The ion beam used for milling was set at 30 keV. The electron beam for imaging was set at 1.55 kV. The 2D image stacks were obtained by using the ion beam for serial sectioning with a slice thickness of 80 nm. The width of the cross-section was 40 μm and the height 25 μm. A backscattered electron detector was used with a pixel size 40 nm.

2.6. Image analysis and 3D reconstruction

From the in-plane CLSM micrographs, the characteristic length scale of the phase-separated structure was estimated using the method described in detail in Carmona et al. (2021). In short, the steps in the Fourier image analysis are to first compute the power spectrum from the micrograph, where each point represents a frequency contained in the real domain image. Second, an intensity peak that represents the dominant frequency in the Fourier space is showing the characteristic length scale in the original image. Finally, an estimate of the characteristic length scale L is obtained as $L = FOV/\mu$, with μ being the mean of the radial distribution representing the peak and FOV the field of view of the micrograph in μm.

For the *in situ* CLSM experiments, ImageJ/Fiji was used to manually estimate the thickness of the film (Schindelin et al., 2012).

For the rest of the experiments, the thickness of the films was estimated by localizing the upper and lower surface of the film, allowing film thickness estimation at each time point using MATLAB (Mathworks, Natick, MA, USA), as described in Carmona et al. (2022b).

From the xyz-CLSM micrograph series and the FIB-SEM data, it was possible to perform a 3D visualization with built-in plugins in Fiji/Image J called *Volume Viewer* and *3D viewer* as described in Schmid et al. (2010).

2.7. Simulation of the structure evolution during layer formation

We simulated simultaneous ethanol evaporation and spinodal decomposition taking place during the formation of a multilayer EC/HPC film. In the following sections, for clarity, we solely display the key elements and equations which form the basis for the simulation. A detailed description of the simulations can be found in the supporting material.

2.7.1. Modelling of a three-component system undergoing both evaporation and spinodal decomposition using the Cahn-Hilliard equation

The simulation was based on the Cahn-Hilliard equation as we assumed that the phase separation and mixing are governed by diffusion only (Cahn, 1965). We adopted the so called fast mode model for the flux expressions as proposed by Kramer et al. (1984) and displayed in Eqs. (S1) and (S2) in the supporting material.

2.7.2. Initial conditions for simulation

The simulation considers an ethanol droplet containing a small amount of EC polymer, placed on top of a dry phase-separated EC/HPC layer. The combined system is subsequently allowed to evaporate. The dried EC/HPC film contains 45 wt% HPC. We consider a 2D system in the simulations.

To construct the initial phase-separated EC/HPC domain, we performed a Cahn-Hilliard simulation of the spinodal decomposition taking place in an EC/HPC mixture containing 10 vol% ethanol (Eqs. (S11), (S12) and (S13)). The thickness of one layer of EC/HPC is obtained from inspecting the experimental CLSM micrograph in Fig. 6, Section 3.2.1. The second EC/HPC domain with 45 wt% HPC made up of five layers in Fig. 6 is seen to have a thickness of 22 μm, giving a layer thickness of

about 4.4 μm (see also Fig. S1). The film width in the simulation was chosen to be 2.5 μm. The added ethanol-polymer layer was represented as 2.5 μm × 75 μm and containing 4 vol% (equal to 6 wt%) EC polymer (refer to Section 2.2 "Construction of EtOH-EC liquid domain" in the supporting material).

2.7.3. 2D simulation of EtOH evaporation from an EC/HPC/EtOH mixture

When the two layers are brought together, many phenomena are taking place; here we considered the evaporation of the total structure from Section 2.7.2. We assumed an evaporation rate of 17 μm/sec. As the evaporation proceeds, the polymer volume fraction at the film surface increases and the evaporation rate decreases.

This phenomenon is mimicked by multiplying the evaporation rate by a factor proportional to the ethanol vapor pressure which is evaluated by Flory-Huggins theory (Flory, 1942). The equations we solve are based on the polymer flux expressions derived from Kramer's theory of interdiffusion (Kramer et al., 1984). The main equations used in the simulation are Eqs. (1), (2) and (3), corresponding to Eqs. (S14), (S15) and (S16) in the supporting material, respectively.

Eq. (1) is based on the free energy form of the Flory-Huggins theory (Flory, 1942):

$$\dot{\psi} = k_g T \Delta\rho B \left\{ \frac{1}{2N_B} \ln\frac{\rho+\psi}{2} - \frac{1}{2N_A} \ln\frac{\rho-\psi}{2} - \frac{\chi_{AB}}{2}\psi - \kappa\Delta\psi + \eta(t) \right\} \quad (1)$$

$$- \nabla\left(\frac{\psi}{\rho}\right)\cdot J_\rho + \frac{\psi}{\rho}\dot{\rho}$$

Here, ψ is the order parameter defined below, k_B the Boltzmann's constant, T the temperature, ρ the total polymer volume fraction, B is the polymer segment mobility, N_B and N_A are the lengths of HPC and EC polymers, respectively, χ_{AB} is the polymer–polymer Flory–Huggins parameter, κ is the interfacial interaction parameter, $\eta(t)$ is a small noise term needed to induce phase separation in the spinodal region, and J_ρ is the total polymer flux.

$$\dot{\rho} = D_{bin}(\rho)\Delta\rho \quad (2)$$

$$\psi = \varphi_B - \varphi_A, \rho = \varphi_B + \varphi_A \quad (3)$$

Here, φ_A and φ_B are the compositions of EC and HPC, respectively.

In the simulation, we utilized an implementation of the first term of Eq. (1) known as the "cell model" of the Cahn-Hilliard equation (Cahn, 1965). For more detail about the "cell model" see Section 3.2 "Cell model implementation" in the supporting material. In this model, the evaporating film is divided into a fine mesh of cells which holds time-dependent values of ψ and ρ. At each time step of the simulation, the values of ψ and ρ are updated in all cells (refer to equations S21 to S31 in the supporting material).

3. Results and discussion

The aims of this work were to mimic the industrial spraying process and to understand the structure evolution when the layers of the film interact. To characterize multilayer film structures, films had to be produced in a controlled and reproducible manner. In previous work, spin-coating was used to deposit a monolayer of EC/HPC on a glass substrate and the evolution of the phase-separated structure was characterized (Carmona et al., 2021, 2022a, 2022b). The effect of the spin-coating parameters was investigated (Carmona et al., 2021) and the influence of the EC/HPC ratio on the structure evolution during phase separation was extensively discussed (Carmona et al., 2022a, 2022b). In this work, we are investigating the effects of spin-coating parameters and EC/HPC ratio on monolayer and on multilayer EC/HPC films produced by spin-coating. The experimental results are combined with Cahn-Hilliard simulations to analyze the mixing behavior.

3.1. Multilayer films with similar EC/HPC ratio and spin speed

Fig. 5 displays 4 8-layer films produced using 4 different experimental conditions. The EC/HPC ratio and the spin speed are kept constant in each multilayer film. Polymer solutions with either 30 wt% or 45 wt% HPC were deposited onto a glass petri dish and the spin speed was set at either 2000 or 8000 RPM. Each type of film was produced and characterized at least three times. The films were made using the spin-coating process explained in Section 2.2. The formation of the multilayer films displayed in Fig. 5 consisted of 8 deposition cycles, to finally obtain an EC/HPC phase-separated film with 8 layers. Fig. 5a shows the characteristic length scales obtained by Fourier image analysis (see Section 2.6) as a function of height in the film. The image analysis was performed on the in-plane (xy-plane) micrographs (one micrograph every 0.21 μm in the sample as used in Carmona et al. (2021, 2022a). Fig. 5b, c, d, and e show cross-sectional micrographs (xz-plane) of one of the replicates of the film for each experimental condition.

By analyzing the cross-sectional micrographs, it appears that at 2000 RPM the structure of the films obtained with 30 wt% HPC (see Fig. 5b) exhibits bigger structures than the ones obtained with 45 wt% HPC (see Fig. 5c). In addition, the films spun at 2000 RPM exhibit bigger structures than the ones spun at 8000 RPM. These observations are in accordance with previous work (Carmona et al., 2021, 2022a). However, for the films spun at 8000 RPM, bigger structures were obtained with 45 wt% HPC compared to the structures obtained with 30 wt% HPC (Fig. 5d and 5e).

The total thickness h of the film corresponds to the last point of each data set in Fig. 5a. h = 8,12,13, and 16 μm for 30 wt% HPC – 8000 RPM, 45 wt% HPC – 8000 RPM, 30 wt% HPC – 2000 RPM and 45 wt% HPC – 8000 RPM, respectively. By examining the thickness of the film, it is possible to see the influence of both the HPC fraction and the spin speed on the thickness of the film: the overall thickness of the multilayer film is increasing with increasing HPC fraction and decreasing spin speed. This is in accordance with the results found by Carmona et al. (2021), where they could estimate the spinning curves of the EC/HPC system showing that with higher spin speed, a thinner film, and smaller characteristic length scale were obtained. In addition, from their viscosity measurements of EC/HPC solutions, Carmona et al. (2021) showed that the viscosity was increasing with increasing HPC fraction. The increase in film thickness with increasing HPC/EC fraction was explained by the increase in viscosity.

In the cross-sectional micrographs in Fig. 5b, c, d, e it can be observed that there is a gradient in domain size ranging from bigger structures at the substrate surface to smaller structures at the air surface. The same trend is also observed in Fig. 5a. Fig. 5a shows that the average value of the characteristic length scale is decreasing from the substrate surface to the air surface for all the 4 different experimental conditions. The presence of this gradient in structure size can be explained by partial redissolution. In this work, partial redissolution is defined as when introducing new polymer solution during successive deposition cycles, the ethanol contained in the solution penetrates the film and softens the dried polymer film. During the ethanol penetration, the film swells and the mobility of EC and HPC in the preceding layers increases, and the structure that was trapped after solvent quenching can continue to coarsen. The layers closer to the substrate undergo partial redissolution a larger number of times than the layers close to the surface. This results in a gradient in structure size throughout the film, with larger structures in the bottom layers compared to the top layers, because of increased coarsening. The more advanced stages are also supported by the presence of secondary phase separation that is visible inside the layers close to the substrate surface. The secondary phase separation is particularly visible in Fig. 5b, where small domains of EC appear in bigger domains of HPC, and vice-versa. The length scale of the secondary phase separation is significantly smaller compared to the length scale of the primary phase separation (Tanaka and Araki, 1998; Tanaka, 1994).

In Fig. 5b, c, d, and e, it can be noted that for all films, the structure of

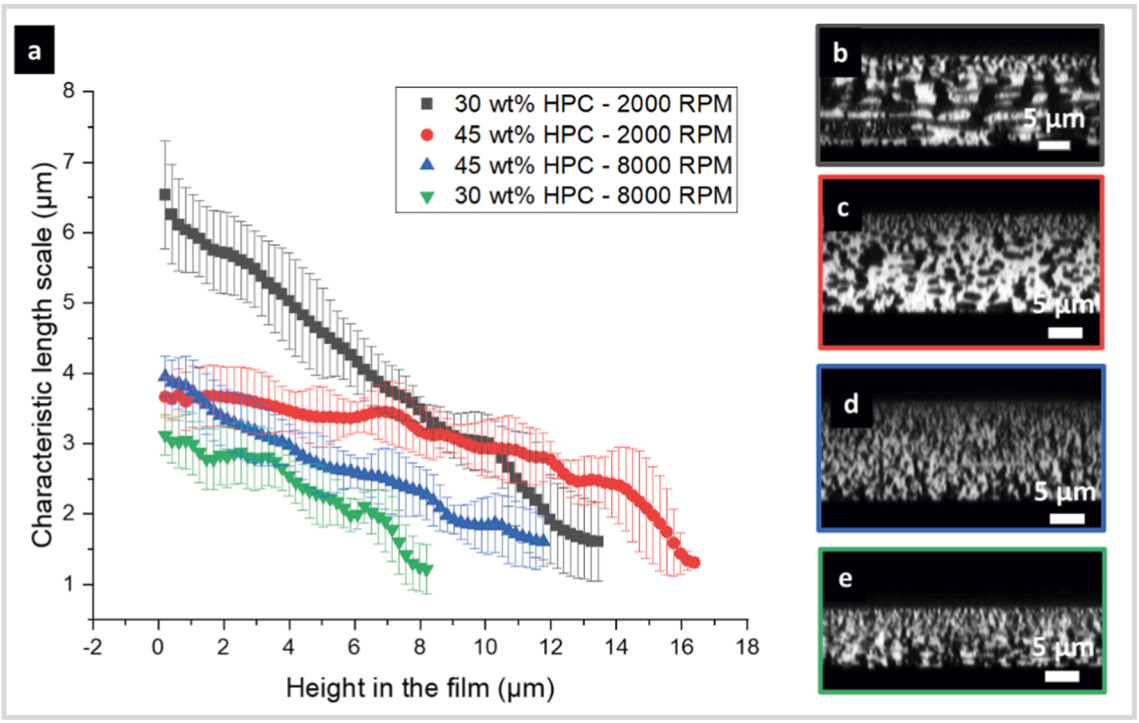

Fig. 5. Influence of EC/HPC ratio and spin speed on 8-layer multilayer films with a) the average value of the characteristic length scale ($m \pm sd$) ($3 \leq n \leq 5$) in the film for the 4 conditions obtained with Fourier image analysis. The micrographs in b) c) d) and e) show the corresponding CLSM-cross sections with b) 30 wt% HPC, 2000 RPM, c) 45 wt% HPC, 2000 RPM, d) 45 wt% HPC, 8000 RPM and e) 30 wt% HPC, 8000 RPM. The bottom part of each cross section is the surface to the substrate and the top part the surface to the air. HPC is bright and EC is dark. On the x-axis in a) 0 height corresponds to the substrate.

the very last layer is particularly small. The measurements in Fig. 5a show that the length scale for the final layer closest to the air is around $L \sim 1$ *to* 2 μm for all 4 film conditions, which is in the same order as the length scale found in monolayers by Carmona et al. (2021). This was also observed by Gebäck et al. (2015), where they found that the top part of an EC/HPC leached film has significantly smaller pore size than the rest of the film.

The observations made on the multilayer films are in accordance with the conclusions made in monolayer films in our previous work (Carmona et al., 2021, 2022a, 2022b). Hence, we assume that the

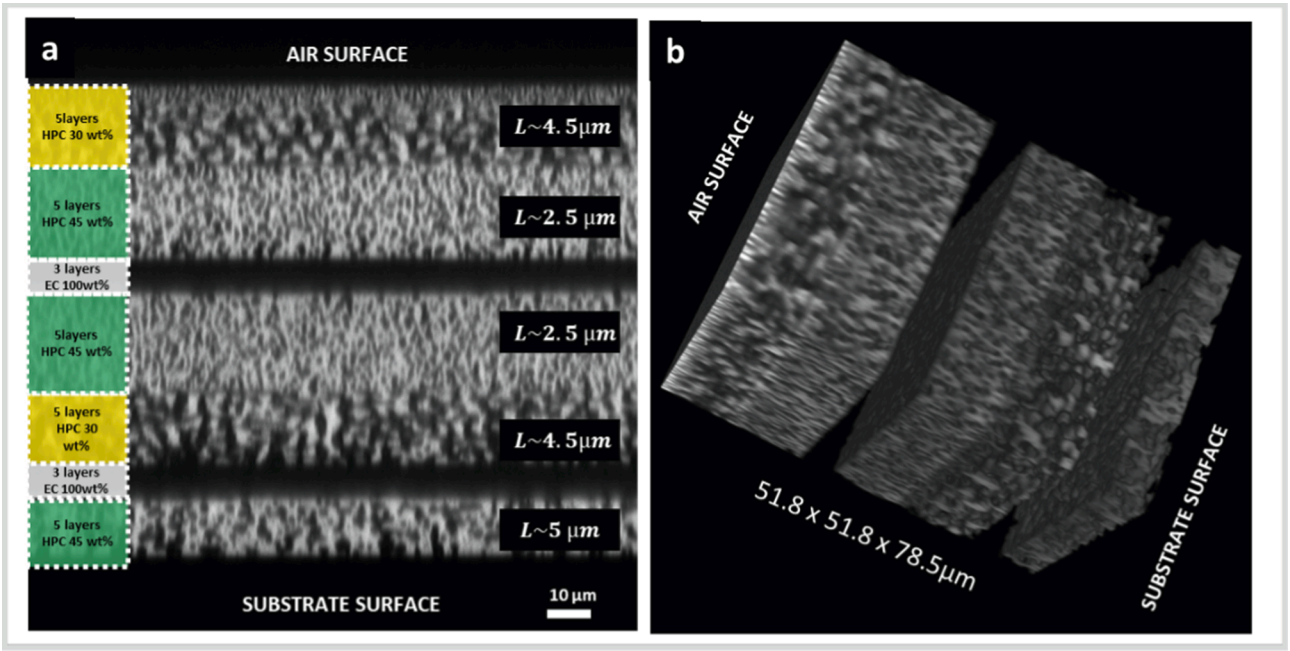

Fig. 6. A multilayer film made of 31 layers, where the EC/HPC ratio was varied between 30 wt% HPC, 45 wt% HPC and 100%wt EC. a) the CLSM cross-section of the film with indication of the EC/HPC ratios used for the layers and the average length scale L in the group of layers obtained with Fourier image analysis. HPC is bright, EC is dark. b) 3D reconstruction of the same film obtained in a volume of 52 × 52 × 79 μm. The image is extracted from Fiji/ImageJ 3D viewer plugin. HPC is solid and EC is hollow.

multilayer films we produce are a superposition of monolayers. However, even though differences are visible between the layers, it is sometimes difficult to identify a clear boundary.

3.2. Obtaining a layered structure by changing the EC/HPC ratio in multilayered EC/HPC films

Fager et al. revealed that the structure of the film coated onto the pellets made through the industrial process of fluidized bed spraying was layered. Boundaries were visible between layers exhibiting different porosity (Fager, 2020). One of the aims of this work was to understand the origin of the layering. It was shown in previous work that the EC/HPC ratio has a strong influence on the structure evolution during phase separation and the final structure (Carmona et al., 2021, 2022a, 2022b). In this section, multilayer films were produced with varying EC/HPC ratio during the successive deposition cycles.

3.2.1. The influence of the EC/HPC ratio on groups of layers

Fig. 6 shows an example of a multilayer film with 31 layers, where the EC/HPC ratio was varied between 30 wt% HPC, 45 wt% HPC and 100%wt EC. The spin-coating process employed follows the method outlined in the material and methods section. During the second step of the process, when the film formation occurs, the spin speed was set at 2000 RPM. In Fig. 6a, a CLSM cross-section micrograph is shown, with indication of the layers deposited during the spin-coating process. In addition, the estimations of the characteristic length scale in a group of layers with the same EC/HPC ratio are also shown. Fig. 6b displays a 3D reconstruction of the same cross-section as shown in Fig. 6a.

It can be seen in Fig. 6a that the boundary between each single layer is difficult to identify when the HPC concentration is the same (similar to the results in Fig. 5). The structure within a group of layers exhibits the same kind of structure: with an almost constant length scale within the group of layers. However, the boundary between groups of layers when changing the EC/HPC ratio is sharp. In particular, the boundary between 100 wt% EC and phase-separated EC/HPC is sharp in both Fig. 6a and b. It is also possible to see the effect of partial redissolution, in the group of 5 layers of 45 wt% HPC at the substrate surface, where the length scale of the phase-separated structure is bigger than close to the air surface. The first group of 45 wt% HPC exhibits a length scale of $L \approx 5\mu m$ which is twice the length scale of the second and third groups ($L \approx 2.5\mu m$). This is an indication that the layers have undergone partial redissolution many times, leading to coarsening of the structure, similar to the results showed in Fig. 5.

Based on the observations in Fig. 6, it seems that the newly introduced layer does not mix with the already existing layers. In addition, even though it is difficult to identify single layers, it seems that the ethanol penetrated the multilayer film and partially redissolved the layers underneath, resulting in a more advanced stage of coarsening and larger structures in the bottom layers. However, it seems that above a certain thickness the amount of ethanol penetrating the film is not

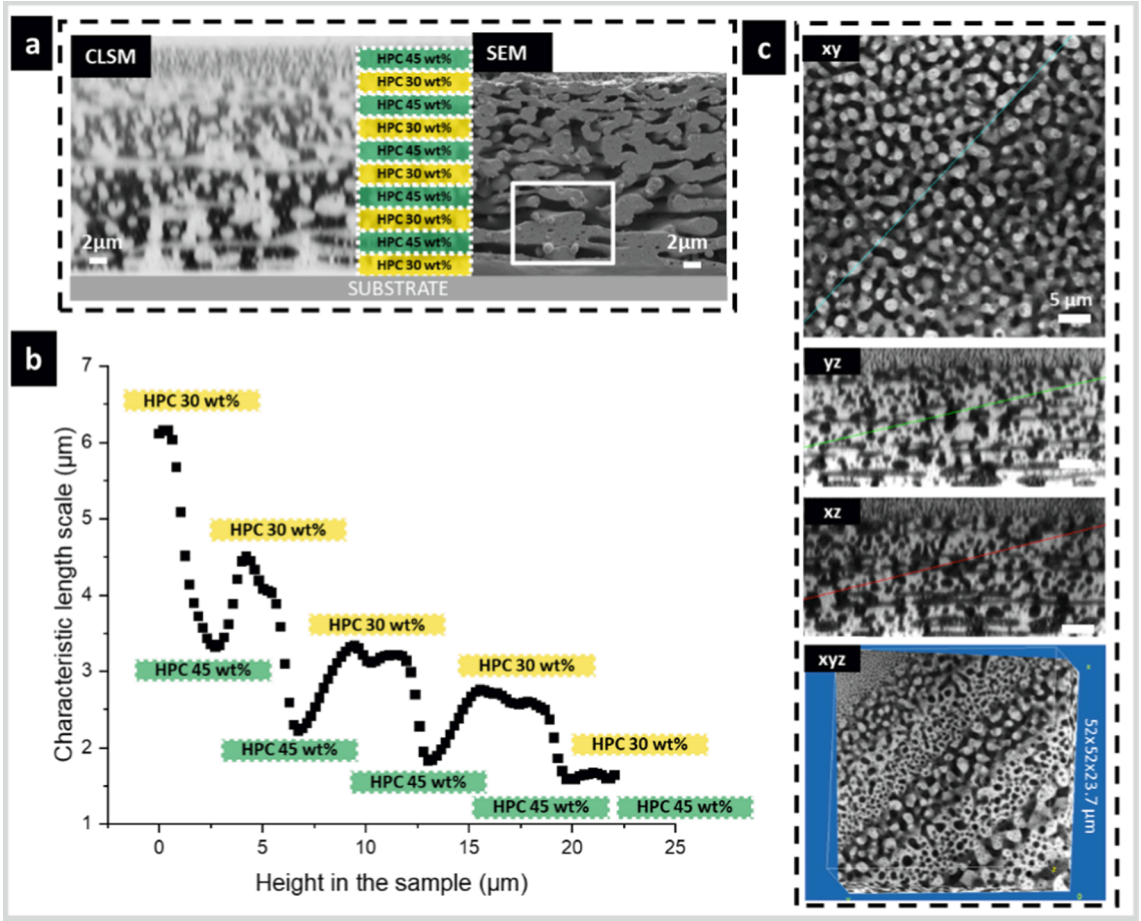

Fig. 7. Characterization of a multilayer EC/HPC film made of 10 layers alternating between 30 wt% and 45 wt% HPC, with a) film cross-section in the xz-plane with the corresponding HPC fraction indicated for each layer. A CLSM micrograph with HPC in dark and EC in bright on the left and a SEM micrograph of the cross-section obtained with a cryostat after leaching of HPC on the right. Secondary phase separation in the EC phase is visible in the SEM image, as indicated by the white rectangle. b) The length scale obtained with Fourier image analysis is plotted versus the height in the sample, 0 μm corresponds to the surface at the substrate. c) Four CLSM sections of the film are shown in the xy, yz, and xz-plane; xyz is the cut of the 3D volume according to the colored lines shown in the xy, yz and xz images. HPC is bright and EC is dark in Fig. 7c. The height in the film corresponds to the z direction.

enough to induce a partial redissolution that would allow coarsening. The thickness of the film and the amount of ethanol in the new layer seem to influence the amount of ethanol that reaches the layers underneath.

3.2.2. The influence of the EC/HPC ratio on alternating layers

In Fig. 7, the same type of approach as in Fig. 6 was used to produce a multilayer film, but where the EC/HPC ratio was alternated for each layer. A 10-layer film was produced by alternating between 30 wt% HPC and 45 wt% HPC. The spin-coating process employed follows the method outlined in the material and methods section. During the second step of the process, when the film formation occurs, the spin speed was set at 2000 RPM. In Fig. 7a, the film cross-section was imaged with CLSM and SEM. In the middle of Fig. 7a, the ratio EC/HPC of the polymer solution that was deposited during the spin-coating production is indicated. It is possible to recognize the gradient in structure size when examining the CSLM and the SEM cross-section micrographs with bigger domains closer to the substrate and smaller domains closer to the air surface. It should be noted that on the SEM cross-section the very last layers with the smaller structure at the top got removed during the leaching process (the cross-section was leached out during 24 h in MilliQ water).

The trend for the change of the domain size observed in Fig. 7a is evident also in Fig. 7b. Fig. 7b is showing the in-plane characteristic length scale in the film obtained with Fourier image analysis. The height $h = 0\mu m$ in the sample corresponds to the substrate surface while $h = 22\mu m$ corresponds to the air surface. The general trend is that the length scale is decreasing from $L(h = 0) \sim 6.2\mu m$ on the substrate surface to $L(h = 22) \sim 1.5\mu m$ on the air surface. As mentioned previously, the partial redissolution makes it possible for the phase separation to reach more advanced stages, leading to bigger structures in the layers deposited first. In this case, we assume that the ethanol penetrates the whole film, *i.e.* the first layer underwent partial redissolution 9 times. The length scale in the last layers is significantly smaller than in the rest of the film, as observed in Fig. 5 and Fig. 6 and in Gebäck et al. (2015). It is also in the order of the length scale observed for monolayer of EC/HPC films spin-coated at 2000 RPM for 45 s in Carmona et al. (2021).

As in Fig. 6, it seems difficult to visually identify single layers in the cross-sections in Fig. 7a. However, when comparing the length scale throughout the film in Fig. 5a obtained by Fourier image analysis, where the EC/HPC ratio was constant, and the length scale through the film in Fig. 7b obtained by Fourier image analysis, where the EC/HPC ratio changes, we see the influence of alternating EC/HPC ratio. In Fig. 7b, an alternation between bigger and smaller structures is observed. This observation is confirmed by the results shown in Fig. 7c. Fig. 7c shows planes in the xy, yz, and xz directions and finally a cut of the xyz volume. The direction of the cut is indicated in the images of xy, yz, and xz-planes. In the xy-plane cut (in a 30 wt% HPC) the length scale seems constant, and a bicontinuous structure similar to the one observed in previous work with films made with 30 wt% HPC is found (Carmona et al., 2021, 2022a, 2022b). The sections in the xz-plane and yz-plane exhibit similar structures as in Fig. 7a. However, in the cut of the volume xyz it is easier to see the transition between the layers made by alternating the EC/HPC ratio. Note that the direction of the xyz cut amplifies the differences between the different layers. We can observe larger structures that would correspond to the layers made with 30 wt% HPC and smaller structures that would correspond to the layers made with 45 wt% HPC.

In the white square in the SEM micrograph in Fig. 7a, secondary phase separation can be seen. This is particularly visible in the bright domains of EC, where smaller domains of leached HPC are observed. The size of the secondary phase-separated domains is significantly smaller compared to the characteristic length scale of the layer, as observed in Figs. 5 to 7 (Tanaka and Araki, 1998; Tran et al., 2006). In the case of EC/HPC coating, when the pellet goes through the spraying zone, the ethanol from the polymer solution hitting the surface of the pellet will penetrate through the phase-separated dried film. It is possible to imagine that the partial redissolution of the polymers is in favor of deepening the solvent quench, making the secondary phase separation visible.

3.2.3. The influence of the EC/HPC ratio characterized with FIB-SEM

Fig. 8 shows a FIB-SEM tomography reconstruction of a leached multilayer EC/HPC film made of 13 layers obtained by varying the EC/HPC ratio between 30 wt% HPC, 45 wt% HPC and 100 wt% EC. Fig. 8a shows the production of the film and the sequence of the different EC/HPC ratios that were used to produce the film. The spin-coating process employed follows the method outlined in the material and methods section. During the second step of the process, when the film formation occurs, the spin speed was set at 2000 RPM. Since the substrate was changed compared to the previous films, we decided to include a carbon tape to avoid charging and to coat this carbon tape with two layers of 100 wt% EC. Fig. 8b and c show the 3D structure obtained by FIB-SEM tomography. In this image, it is difficult to identify the single layers, but we are observing the last 7 layers, before the two layers of pure EC, since there is no leaching under the layers of pure EC.

By analyzing the 3D volume layer by layer, we observed that the pores form a bicontinuous structure through the sample from the top surface, down to the 100 wt% EC layers (see Fig. 8). When a new layer is added, since the system will try to minimize the interface between EC and HPC, the EC and HPC domains in the new layer tend to connect to the already present EC and HPC domains, respectively. This enhances the tendency for the EC domains and HPC from successive layers to be connected, which favors the formation of bicontinuous structures throughout the film with layers exhibiting different porosity. It was observed in previous work that the structure of 45 wt% HPC will form discontinuous-like structure through spinodal decomposition followed by percolation-to-cluster transition (PCT) in monolayer films when allowed to coarsen for several minutes (Carmona et al., 2022). Here, the films are spun for one minute and the structure is trapped during the spinning. Due to the fast drying and early trapping, it is likely that PCT is not taking place and that the structure remains interconnected, which also favors formation of bicontinuous structures. In addition, in the layer on the top corresponding to the surface to the air, significantly smaller structures can be observed. These smaller structures in the top layer were also observed in the films in Figs. 5, 6 and 7.

3.3. Structure evolution when a new layer is added to a multilayer film

During the industrial coating process, polymer solution is sprayed onto the surface of the pellet to form a film. By increasing the time spent in the Wurster fluidized bed, the number of passages for each pellet in the spraying zone increases, resulting in a thicker coating (Heinrich et al., 2015). In the following section, the aim was to understand the interaction between a dried multilayer film and a new wet layer. Therefore, a set-up was developed to monitor *in situ* the structure evolution when a droplet of polymer solution interacts with a multilayer film. The multilayer film corresponds to ten passages in the spraying zone and droplets of one-phase polymer solution (6 wt% polymer in ethanol), hitting the film during the eleventh passage. The structure evolution was characterized with CSLM and the thickness evolution during shrinkage was estimated with image analysis.

3.3.1. Structure evolution when a new layer is applied on a dried multilayer film with the same EC/HPC ratio

Fig. 9 shows the structure and thickness evolutions in ten-layer films during shrinkage of the film after the addition of a droplet of the polymer solution with the same EC/HPC ratio as in the film. In Fig. 9a, the shrinkage of the films for 5 different EC/HPC ratios: 22, 30, 37, 45 and 60 wt% HPC, are compared. In Fig. 9b, the cross-sectional structure evolution of a 37 wt% HPC multilayer film during the addition of a droplet with similar EC/HPC ratio is shown. The spin-coating process

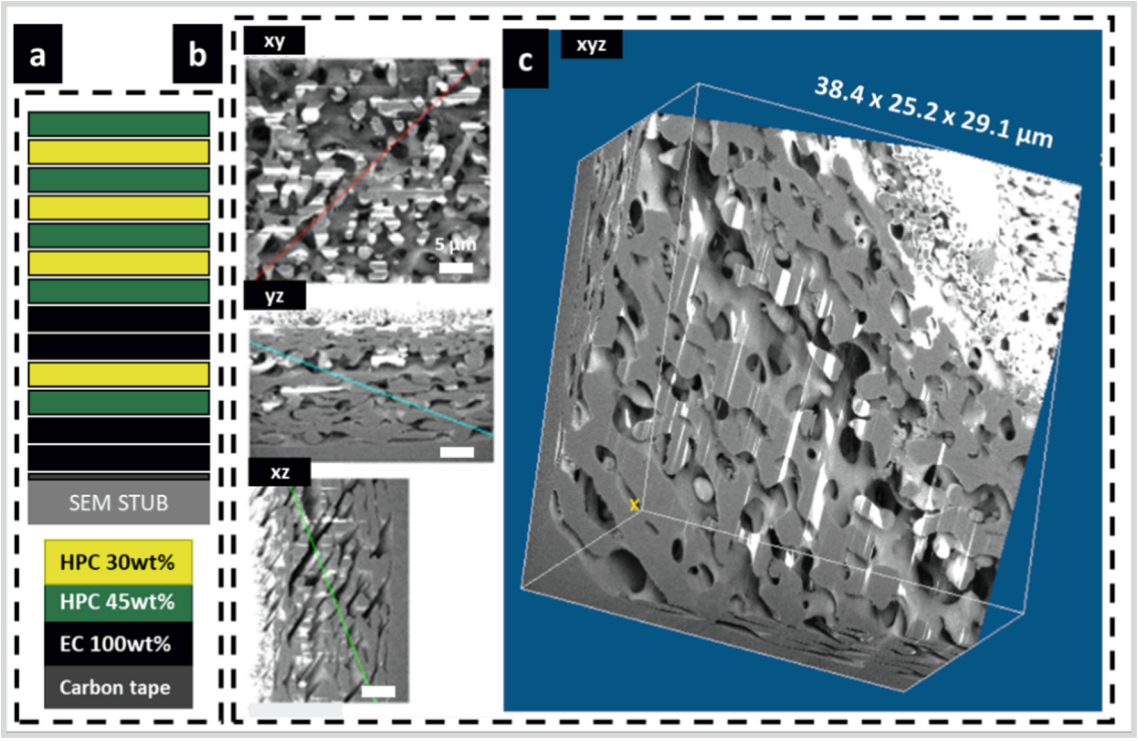

Fig. 8. FIB-SEM Tomography of a multilayer film with varying EC/HPC ratio. a) Schematic illustration of the layer sequences of the film spin-coated at 2000 RPM 1 min + 8000 RPM for extra drying. b) Three FIB-SEM sections are shown of the film in the xy, yz and xz-plane and c) is the corresponding cut of the 3D volume according to the colored lines indicated in the xy, yz and xz images. The grey polymer, having a intensity level corresponds to EC and the pores, correspond to leached HPC.

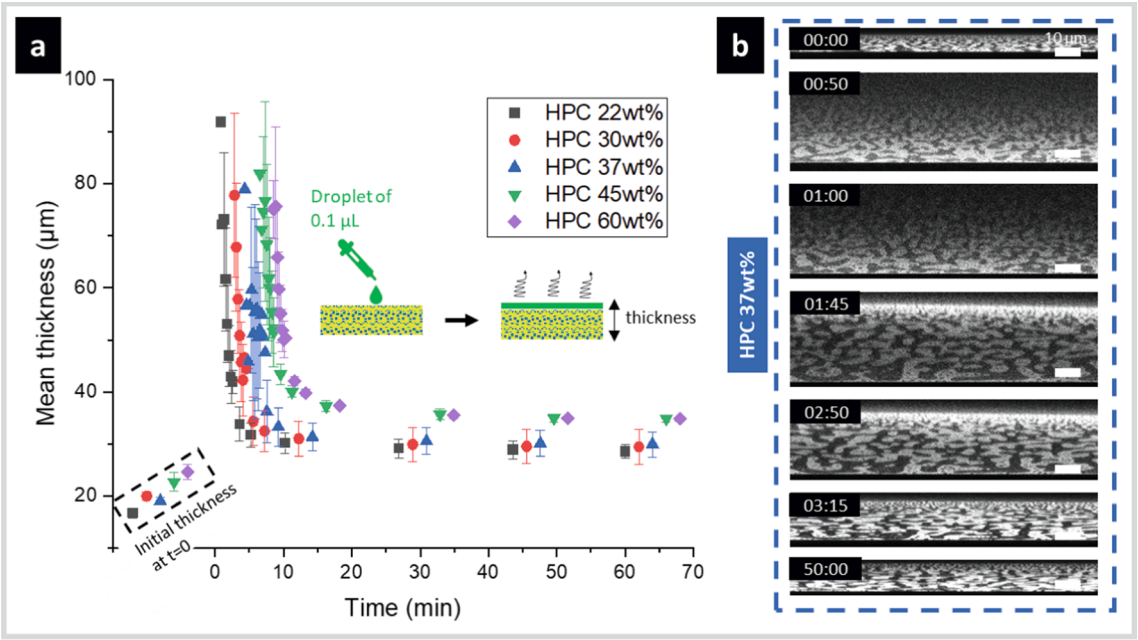

Fig. 9. Thickness evolution of ten-layer films after addition of a 0.1 µL droplet of polymer solution with the same EC/HPC ratio in the film and in the droplet. a) The mean thickness (m ±sd (n = 5) evolution is shown as a function of time for films after droplet addition for 5 different EC/HPC ratios. For better visibility of the data, thickness values are shifted on the x-axis with 0, +2, +4, +6, and + 8 min for 20 wt% HPC, 30 wt% HPC, 37 wt% HPC, 45 wt% HPC, and 60 wt% HPC, respectively. b) Cross sectional micrograph of a 37 wt% HPC 10 layer film with addition of a droplet at t = 25 s. For each micrograph, the time is indicated on the top left. HPC is bright and EC is dark. The lower part is the substrate surface, and the upper part is the air surface where the droplet is deposited.

employed follows the method outlined in the material and methods section. During the second step of the process, when the film formation occurs, the spin speed was set at 2000 RPM.

It should be noted that the scale is much bigger in our experimental set-up compared to the industrial process. In the industrial process of fluidized bed spraying, the size of the droplet is estimated to be

approximately 20μm in diameter while the droplet of 0.1 μL has a diameter of approximately 500 – 600 μm. On average, the addition of the droplet increased the thickness of the film by about 11μm after 60min corresponding to an augmentation of about 100% of the thickness of the film. This means that the time scale and the amount of dissolution is exaggerated compared to the industrial scale.

In Fig. 9a, it can be noted that most of the evaporation happens during the first 10min, which is in accordance with gravimetric studies performed earlier by Carmona et al. (2022a). In addition, the curves follow the same shape and trend for all the 5 ratios, showing that the EC/HPC ratio has negligible influence on the evaporation process. This is in accordance with previous observations made by Carmona et al when the shrinkage rate of a monolayer film in a closed petri dish was found to be independent of the EC/HPC ratio (Carmona et al., 2022a). At around 20min, almost all ethanol from the droplet has evaporated, and a plateau of thickness is obtained. The influence of the EC/HPC ratio on the initial thickness, before the addition of the droplet, is in accordance with the trend observed previously, where the thickness of the film increases with the HPC fraction (Carmona et al., 2021). On average, the initial thickness of the 10-layer films is 17 ± 1 μm, 20 ± 1 μm, 19 ± 1 μm, 23 ± 2 μm, and 25 ± 1 μm for 22, 30, 37, 45, and 60 wt% HPC, respectively. The same trend is visible at the end of the film shrinkage, 60 min after the droplet addition, with a final thickness of 29 ± 1 μm, 29 ± 3 μm, 30 ± 2 μm, 35 ± 1 μm, and 35 ± 1 μm for 22, 30, 37, 45, and 60 wt% HPC, respectively. With increasing HPC fraction, the viscosity of the coating solution increases, and more material remains in the film during the spin-coating process (Carmona et al., 2021, 2022a, 2022b).

Fig. 9b shows an example of the drying of a droplet on a 37 wt% HPC 10 layer film. The droplet with 37 wt% HPC was added at $t = 25s$. In the micrograph at 50s, it is possible to see that the thickness of the film has significantly increased to more than 4 times larger than the initial thickness. After the addition of the droplet, it is likely that the ethanol contained in the droplet (having a large volume compared to the film) is penetrating throughout the whole film. Thus, the 10 layers in the initial film are undergoing partial redissolution *ie.* softening, swelling and coarsening due to increased polymer mobility. It is possible to observe the coarsening in the cross-sectional micrographs (Carmona et al., 2022a, 2022b). It appears that the coarsening mechanism taking place is likely to be hydrodynamic growth for 37 wt% HPC in accordance with previous work (Carmona et al., 2022b).

Before the droplet introduction, the structure was trapped in a certain phase-separated state. After droplet introduction, a much thicker film is formed. Subsequently, the ethanol evaporates and the thickness of the film decreases. When the thickness reaches a plateau at around 10 min, the phase separation is considerably slowing down, and the phase-separated structure is trapped again. However, the length scale in the film is larger in the first 10 layers when comparing the layers before and after the penetration of ethanol. It can also be noted that it is not possible

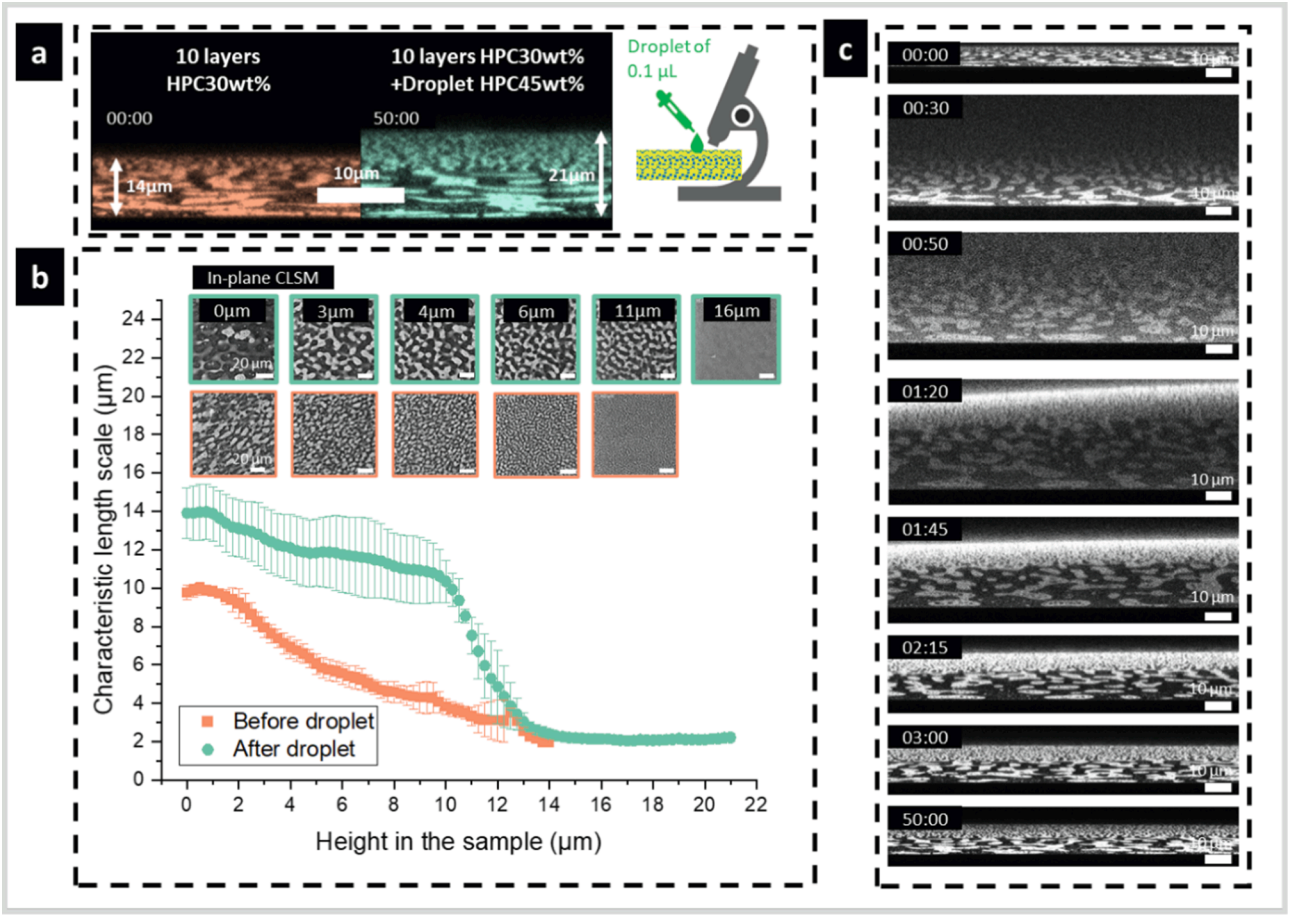

Fig. 10. Interaction between 10-layer films after addition of a droplet of 0.1 μL of a coating solution with a different EC/HPC ratio in the film and in the droplet. a) CLSM cross-section of the multilayer film at t = 0 just before introduction of the droplet and at t = 50 min after the droplet. The estimated film thickness is displayed. On the right, a schematic illustration of the experimental set-up used to follow the structure evolution *in situ*. b) The characteristic length scale (m ±sd(n = 3) through the films is plotted before and after addition of the droplet(t > 60 min). The characteristic length scale is analyzed using Fourier image analysis. Corresponding in plane CLSM micrographs used for the Fourier image analysis are displayed. c) Cross sectional micrograph of a 30 wt% HPC 10 layer film with addition of a 45 wt% HPC droplet at t = 25 s. For each micrograph, the time is indicated on the top left. HPC is bright and EC is dark. The lower part is the substrate surface, and the upper part is the air surface where the droplet is deposited.

to observe any boundary between the multilayer film and the new layer. Finally, as observed previously the structures closest to the air surface exhibit significantly smaller structures. The layer closest to the air is drying faster (Mokarian-Tabari et al., 2010; Raj Kumar, 2012; De Gennes, 2002; De Gennes, 2001; Cummings et al., 2018), so that the phase-separated structure is trapped at an earlier stage, resulting in a smaller structure. Note that the thickness of this air surface layer is much smaller than the thickness of the added layer.

3.3.2. *Structure evolution when a new layer is applied on a dried multilayer film with different EC/HPC ratio*

In the following part, we investigated the interaction between a multilayer film and a polymer solution droplet with a different EC/HPC ratio. Fig. 10 shows an example of the interaction between a multilayer film made of 10 layers of 30 wt% HPC and a 45 wt% HPC 0.1 μL droplet. The spin-coating process employed follows the method outlined in the material and methods section. During the second step of the process, when the film formation occurs, the spin speed was set at 2000 RPM. The same behavior was observed for all three replicates. Fig. 10a shows a CLSM cross-section of the film before and 50*min* after the droplet introduction. Fig. 10b shows the in-plane characteristic length scale through the film obtained by Fourier image analysis, obtained by averaging the length scale at different heights in the sample in three different films. In-plane CLSM micrographs recorded at different depth in a multilayer film before and after droplet addition are also shown in Fig. 10b. Fig. 10c shows the structure evolution of a ten-layer film with the introduction of a new droplet at 25 s.

On the cross-section after the droplet introduction at 50*min* in Fig. 10a, it can be noted that there is a clear boundary between the two groups of layers exhibiting two different morphologies and length scales, which correspond to the boundary between the 10 layers of 30 wt% HPC and the new droplet layer of 45 wt% HPC.

The characteristic length scales shown in Fig. 10b confirm that there is a transition between the 10-layer film and the new layer the height in the sample goes from approximately 10 to 14 μm. With the first original 10 layers from 0 to 10 μm and the droplet layer with an almost constant length scale of $L(h) \sim 2\mu m$ from 14 to 21 μm.

The cross-sectional CSLM micrographs in Fig. 10c show the shrinkage of the film and the structure evolution over time. As observed in Fig. 9, the film is swelling when the droplet is deposited and the ethanol from the droplet penetrates the film. Then, the ethanol is evaporating, and the film is shrinking. While shrinkage of the film is taking place, a clear boundary is appearing already at 1:20 min in Fig. 10c. The ethanol penetration is inducing the partial redissolution of the dried layer and therefore, coarsening. The effect of partial redissolution is particularly visible on the in-plane micrographs in Fig. 10b, where the structure after the droplet is bigger than before the droplet. We observe this coarsening within the multilayer film while the film is shrinking resulting in a bigger length scale in the first 10 layers than in the later ones. As seen in Fig. 10c and confirmed in Fig. 10b, the length scale of the layers from 0 to 10 μm grew with additional 4 μm.

This experiment shows that even with a very large amount of polymer solution deposited onto the surface of the film with the droplets, the ethanol penetrates and softens the polymer material, but the polymers from the successive layers do not mix. The boundary between the 10 layers of 30 wt% HPC and the droplet of 45 wt% HPC is particularly clear in Fig. 10a and 10c. The thickness of the new layer is significantly larger than the fast-drying top layer. Also, the boundary was not clear when adding a droplet of the same ratio (see Fig. 9), although some tendency that EC and HPC of the newly added layer connect to the already present EC and HPC domains could be observed. Thus, HPC domains from the new introduced layer tend to find HPC domains and EC domains tend to find EC domains. This could explain why it is difficult to identify single layers on cross-sections as observed in Figs. 5, 7, and 8. Our hypothesis is that since EC and HPC are immiscible, when they are partially redissolved, they phase separate again within the layer but there is no driving force to mix with the new introduced polymer material from the new layer.

3.3.3. *Simulation of the structure evolution during the deposition of a new layer on a dried multilayer film with different EC/HPC ratio*

From the results shown in Figs. 6, 7, 8, 9, and 10, it seems that when forming multilayer films with sequential spin-coating, the layers in the multilayer EC/HPC films do not mix. When changing the EC/HPC ratio between layers, discontinuities were observed. To investigate these observations in more details, Cahn-Hilliard simulation including the ethanol evaporation process was performed. The focus was on the interaction between two layers during film formation corresponding to the case in Fig. 6, *i.e.* the interaction between a 4.4 μm thick dried phase separated film containing 45 wt% HPC, and a new layer of pure EC and ethanol with a thickness of 75 μm (which corresponds to 3 μm when dried), see also Fig. S1. The detailed method for implementing the simulation can be found in the Supporting Material.

Fig. 11 displays a simulated time-series of a film structure consisting of 45 wt% HPC where a layer with pure EC in ethanol is added on top. The x- and z-axis are in the units of number of simulation cells. Each cell is quadratic, and the length of each side is 0.025 μm. In Fig. 11 a, b, c and d, we consider a sequence of snapshots of the order-parameter $\psi = \phi_{HPC} - \phi_{EC}$ recorded as the simulation proceeds. In Fig. 11a, we show the order parameter before the simulation starts with a zoom of the film inserted. In Fig. 11b, we show the film at an intermediate time (3 s), where 2000 cell layers have evaporated. After having evaporated 2630 cell layers, the polymer volume fraction on the top of the film is very close to unity and the evaporation rate is very slow. The corresponding order-parameter plot is shown in Fig. 11c. Finally, in Fig. 11d, the final film structure is shown. We clearly see a large EC domain on top of the phase-separated structure. This non-mixing behavior corresponds very well with the observed layering between 45 wt% HPC and pure EC seen in Fig. 6a.

An important outcome of the simulation, besides the order parameter shown in Fig. 11 is the total polymer volume fraction, as given by Equation (2) in section 2.7. The value of this quantity determines the extent of spinodal decomposition. It is shown as a function of the position in the film at different time-points for the total film evaporation process in Fig. 12. The first curve labelled "1″ corresponds to the initial state before the evaporation has started. Curve number 2 corresponds to a state just after the start of evaporation. Subsequently, a higher number corresponds to a later stage of evaporation. In Fig. 12, during the whole evaporation process it can be seen that the total polymer fraction of the first ~ 250 layers (which corresponds to the initial thickness of the phase separated film) remains above ~ 0.13 (grey dashed line in Fig. 12), which equals the phase boundary calculated from Flory-Huggins theory. For this reason, during mixing of the layers, partial redissolution of the already present layer is taking place, but not enough for the mixture to leave the spinodal region and become a molecular dispersed solution. Thus, the simulation of the total polymer volume fraction supports the hypothesis that layers do not mix. In the two-phase region, there is no driving force for mixing between an already present layers and a new layer. The simulation results shown in Figs. 11 and 12 and the experimental results shown in Figs. 5–10 clearly show that subsequent layers do not mix.

3.4. *Influence of the spin speed on the multilayer film structure*

Observations in the previous sections indicated that it was likely that during the multiple deposition cycles through the spin-coating process, the successive deposited layers do not mix. In the industrial pellets, it was observed that there are layers that exhibit a varying porosity in the coating (Fager, 2020). Our hypothesis is that since the coating in the fluidized spraying device is rather chaotic, the parameters of the system are varying between each passage in the spraying zone, thus giving rise to different structures in different layers. Many phenomena are taking

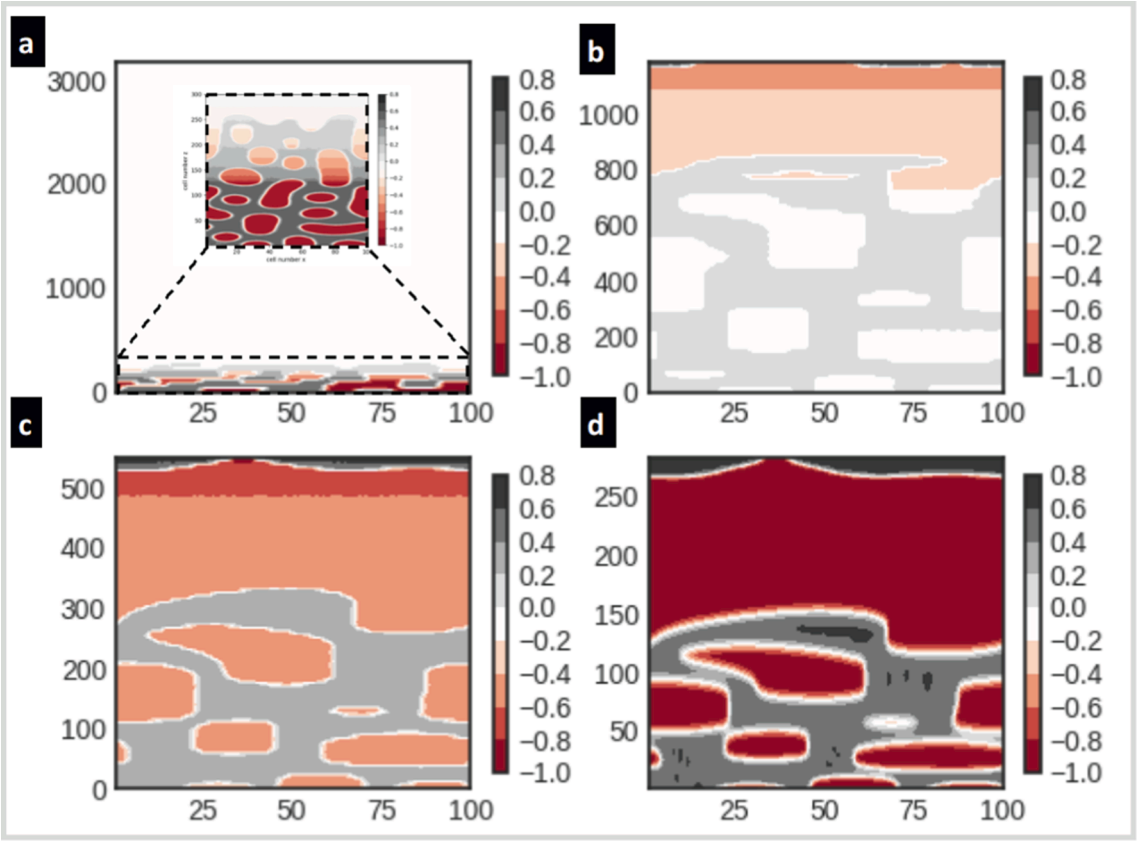

Fig. 11. Simulation of the interaction between a phase-separated film of EC/HPC with 45 wt% HPC and a layer of 100 wt% EC in ethanol. The snapshots display the order parameter $\psi = \phi_{HPC} - \phi_{EC}$ with red ($\psi = -1$ corresponding to the domain of pure EC and black ($\psi = 1$) corresponding to the domains of pure HPC. With the order parameter plot, a) before evaporation b) after 2000 cell layers (corresponding to 50 μm) has evaporated c) after 2630 cell layers (corresponding to 66 μm) has evaporated and d) after full evaporation, corresponding to the final structure. In the top of a) a zoom of the structure is inserted. Note that from one snapshot to another the number of cells on the z-axis varies. a) b) c) and d) can also be found in the supporting material with more details as Figures S4, S6, S7, and S9 respectively. (For interpretation of the references to colour in this figure legend, the reader is referred to the web version of this article.)

place simultaneously, but probably the following three parameters are most likely to influence the porosity for each passage: the pellet process temperature (drying rate), the ethanol content, and the EC/HPC ratio. During spin-coating, the spin speed is directly related to the drying rate and the film thickness. It is, therefore, interesting to investigate the effect of the spin speed on the structure of the multilayer films. It was shown in previous work (Carmona et al., 2021, 2022a, 2022b) and in Section 3.1 that the change of spin speed influences both the layer thickness and the structure length scale. In this section, we investigated the effect of alternating spin speed during the multilayer film production on the film structure.

Fig. 13 shows an example of a ten-layer film made by alternating the spin speed between 2000 RPM and 8000 RPM during the film formation step of the coating process (refer to Section 2.2 for production details). In Fig. 13a, the sequence of the deposition cycle is displayed, and a CLSM cross-section of the film is shown. As for the films in Figs. 5, 7 and 8, it is difficult to identify the single layers. Fig. 13b shows the in-plane characteristic length scale in the film obtained with Fourier image analysis. 0 μm corresponds to the surface to the substrate while 22 μm corresponds to the surface to the air. The general trend is that the length scale is decreasing from the substrate surface, where $L(h) \sim 4.9\mu m$, to the air surface, where $L(h) \sim 1.5\mu m$ is in accordance with the results shown in Figs. 5, 7, 8 and 10. As mentioned previously, the partial redissolution takes place in each deposition cycle and in the layers already deposited, the phase separation is restarted, leading to bigger structures. However, we have a less pronounced gradient compared to the one observed in Fig. 5. An alternation between small and bigger structures can be seen in Fig. 13b, similar to the results in Fig. 7, with a smaller length scale and thinner layers when the spin speed was 8000 RPM and a bigger length scale and thicker layers when the spin speed was 2000 RPM. This observation is in accordance with earlier work (Carmona et al., 2021).

Fig. 13c shows the phase-separated structure in cuts in the 3 planes xy, xz, and yz and finally a cut of the volume xyz. It can be observed on the cut of the volume xyz that smaller and bigger structures alternate because of the alternating spin speed during spin-coating. Note that the cut amplifies the differences between the different layers.

During the multilayer film formation in the industrial fluidized bed spraying device, it is highly likely that many different phenomena are competing, as stated in the introduction section. Based on the results, it seems that the influence of spin speed (drying rate) can partly explain the varying porosity in the industrial pellets.

4. Conclusions

The combination of spin-coating, microscopy (CLSM, SEM, FIB-SEM), simulations, and image analysis was very efficient in characterizing the structure of multilayer, phase-separated EC/HPC films. The results showed that production of multilayer films via spin-coating is well-controlled and reproducible. In addition, it was found to be a good model set-up to mimic and understand the structure formation of EC/HPC coating on pellets in the industrial fluidized bed spraying device. This set-up allowed us to study the influence of EC/HPC ratio and spin speed on the final multilayered phase-separated structure. In addition, it was also possible to follow the structure evolution *in situ* during the addition of a new layer on a multilayer film. Thus, we could investigate

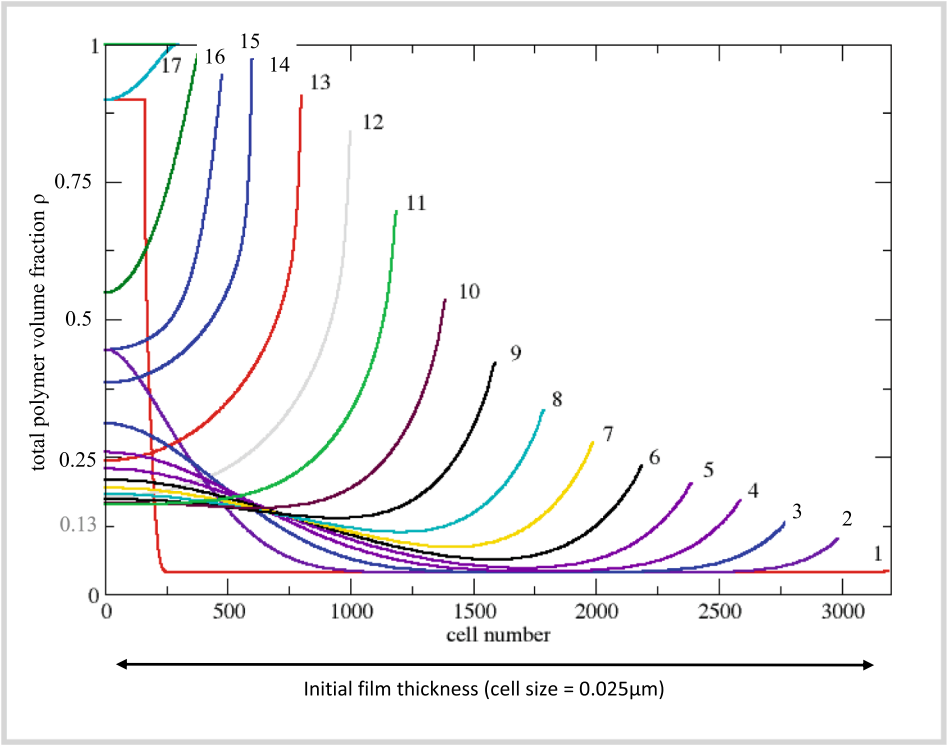

Fig. 12. Total polymer volume fraction in the polymer film, as a function of film thickness for different times in the evaporation process. The curves are numbered from 1 to 17, with curve 1 corresponding to the initial state and 17 to the latest state. The dashed grey line corresponds to a total polymer fraction of 0.13. The figure can be found with more details as Fig. S8 in the supporting material.

our hypotheses: in the industrial coating, there are two main ways for obtaining the multilayered structure: change of spin speed (*i.e.*, drying rate and film thickness) and change of EC/HPC ratio every other layer.

Analysis of multilayer films made at constant EC/HPC ratio and constant spin speed showed that the multiple layers have the same behavior as the monolayers: the film thickness and the characteristic length scale decrease with increasing spin speed. The film thickness increases with increasing HPC fraction. At 2000 RPM the characteristic length scale increases with increasing HPC fraction. In addition, we found the presence of a gradient in structure size with larger structures close to the substrate surface and smaller structures close to the air surface. This gradient can be explained by the partial redissolution of the layers already deposited. Secondary phase separation was visible and confirmed the presence of the partial redissolution and the structure size gradient.

When alternating the EC/HPC ratio between the layers, the different layers exhibited different morphologies and alternation of porosity. The layers could be identified both on the film cross-sections and 3D volumes, made with CLSM, SEM cross-section and FIB-SEM tomography.

From the *in situ* CLSM experiments, when a droplet of polymer solution was deposited onto a multilayer film, it was shown that layers do not mix. There is no driving force for the polymers on superposed layers to mix since they are immiscible. The different layers do not mix but EC and HPC domains in the newly added layer tend to connect to the EC and HPC domains in the already present structure and thus no abrupt changes (or discontinuities) at the interface between two layers could be observed. The observation that layers do not mix was supported by a Cahn-Hilliard simulation of the phase separation process with simultaneous ethanol evaporation.

Finally, by varying spin speed in each deposition cycle, a layered film with varying porosity could be obtained. We propose that the change of spin speed during the coating process is one of the possible explanations for the changes in porosity: the drying rate of the pellet for each passage in the spraying zone varies forming layers with different porosity.

This study of the multilayer EC/HPC films gives valuable insights into the structure formation and the origins of the layered structure in the industrial EC/HPC pellet coating. To further explore the structure formation in the industrial process, it would be of interest to investigate the structure evolution *in situ* during the interaction between an EC/HPC multilayer film and droplets of equivalent size as in the fluidized bed spraying device.

CRediT authorship contribution statement

Pierre Carmona: Conceptualization, Methodology, Software, Formal analysis, Investigation, Writing – original draft, Writing – review & editing, Visualization. **Jens Poulsen:** Methodology, Software, Formal analysis, Investigation, Resources, Data curation, Writing – review & editing, Visualization. **Jan Westergren:** Methodology, Formal analysis, Resources, Data curation, Writing – review & editing. **Torben Nilsson Pingel:** Methodology, Investigation, Visualization, Writing – review & editing. **Magnus Röding:** Methodology, Software, Formal analysis, Resources, Data curation, Writing – review & editing, Supervision. **Eileen Lambrechts:** Validation, Investigation. **Herlinde De Keersmaecker:** Validation, Investigation, Resources, Writing – review & editing, Supervision. **Kevin Braeckmans:** Writing – review & editing. **Aila Särkkä:** Writing – review & editing, Supervision. **Christian von Corswant:** Conceptualization, Writing – review & editing, Supervision, Funding acquisition. **Eva Olsson:** Writing – review & editing, Supervision. **Niklas Lorén:** Conceptualization, Writing – review & editing, Supervision, Project administration, Funding acquisition.

Declaration of Competing Interest

The authors declare that they have no known competing financial interests or personal relationships that could have appeared to influence the work reported in this paper.

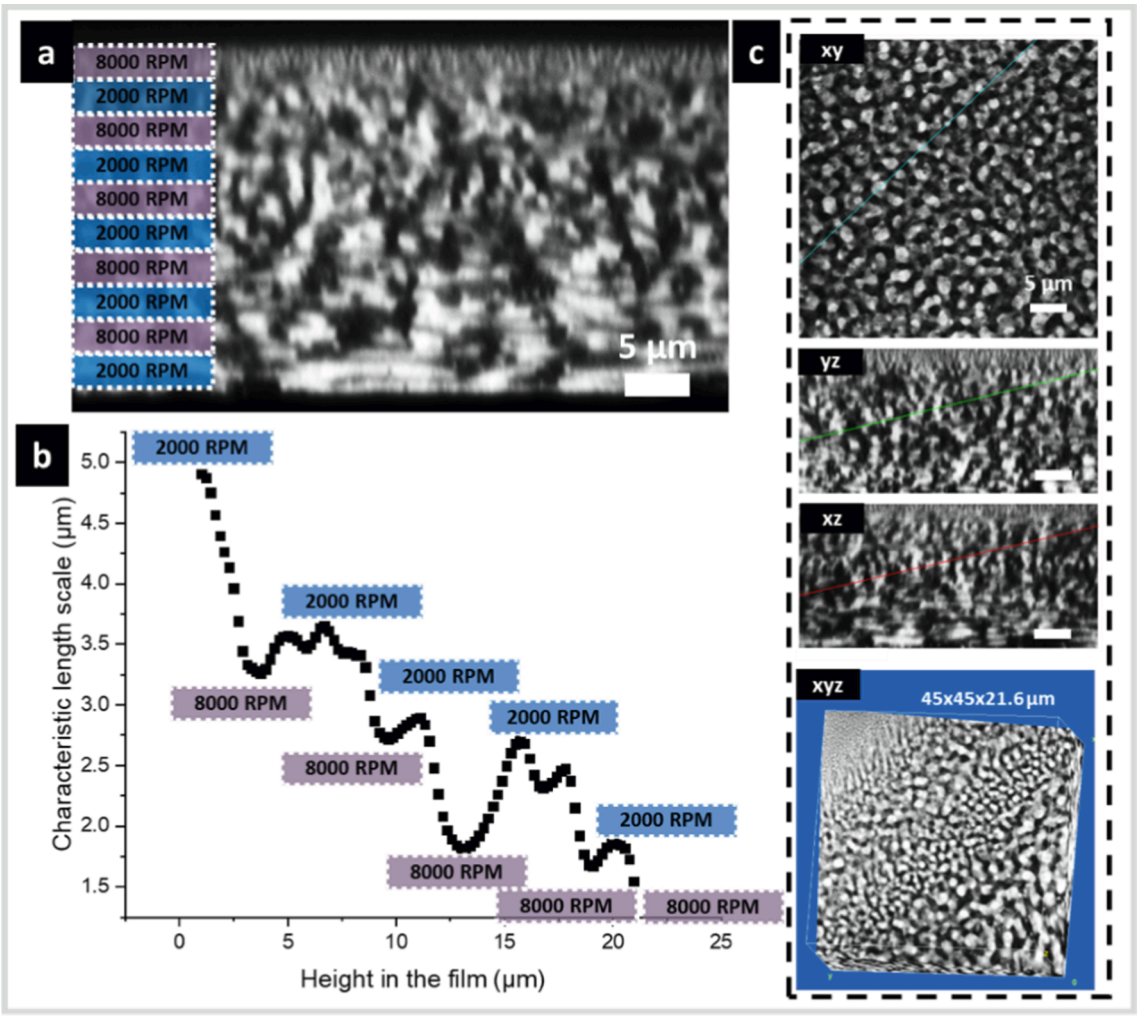

Fig. 13. Characterization of a multilayer EC/HPC film made of 10 alternating layers of 30 wt% HPC produced by 2000 RPM and 8000 RPM spinning. a) A CLSM cross-section in the xz-plane of the film with the corresponding spin speed for each layer indicated. b) The characteristic length scale obtained with Fourier image analysis from the in-plane CLSM micrographs versus the height in the sample. 0 µm is the surface at the substrate and 22 µm is the air surface. c) Three sections of the film in the xy, yz and xz-planes, and the xyz section which is the corresponding cut of the 3D volume. HPC is bright and EC is dark. The height in the film corresponds to the z direction.

Data availability

Data will be made available on request.

Acknowledgements

The Swedish Foundation for Strategic Research (SSF grant FID16-0013), the Swedish Research Council (VR grant 2018-03986), and the Swedish Research Council for Sustainable Development (grant 2019-01295) are gratefully acknowledged for the funding. AstraZeneca is acknowledged for the financial support and materials. Funding is acknowledged by the Fund for Scientific Research Flanders (grants I012020N & I000321N) and the Special Research Fund of Ghent University (grant BOF.COR.2022.0003.01). Dr. Cecilia Fager is acknowledged for fruitful discussions about FIB-SEM imaging of EC/HPC films.

Appendix A. Supplementary data

Supplementary data to this article can be found online at https://doi.org/10.1016/j.ijpharm.2023.123350.

References

Alig, I., Rüllmann, M., Holst, M., Xu, J., 2003. Phase separation by continuous quenching: similarities between cooling experiments in polymer blends and reaction-induced phase separation in modified thermosets. Macromol. Sympos. 198 (1), 245–258.

Andersson, H., 2015. Structure Control by Phase Separation and Influence on Mass Transport in Films for Controlled Release. Chalmers Universit of Technology, Gothenburg, Sweden, Department of Materials and Manufacturing Technology.

Ashland, Klucel hydroxypropylcellulose, Physical and Chemical Properties, 2017.

Buxton, G.A., Clarke, N., 2007. Ordering polymer blend morphologies via solvent evaporation. Europhys. Lett. 78 (5), 56006.

Cahn, J.W., 1965. Phase separation by spinodal decomposition in isotropic systems. J. Chem. Phys. 42 (1), 93–99.

Cahn, J.W., Hilliard, J.E., 1958. Free energy of a nonuniform system. I. Interfacial free energy. J. Chem. Phys. 28, 258.

Carmona, P., Röding, M., Särkkä, A., Von Corswant, C., Olsson, E., Lorén, N., 2021. Structure evolution during phase separation in spin-coated ethylcellulose/hydroxypropylcellulose films. Soft Matter 17, 3913–3922.

Carmona, P., Von Corswant, C., Röding, M., Särkkä, A., Olsson, E., Lorén, N., 2022a. Cross-sectional structure evolution of phase-separated spin-coated ethylcellulose/hydroxypropylcellulose films during solvent quenching. RSC Adv. 12 (40), 26078–26089.

Carmona, P., Roding, M., Sarkka, A., von Corswant, C., Olsson, E., Loren, N., 2022b. Structure formation and coarsening kinetics of phase-separated spin-coated ethylcellulose/hydroxypropylcellulose films. Soft Matter 18, 3206–3217.

Cerclier, C., Cousin, F., Bizot, H., Moreau, C., Cathala, B., 2010. Elaboration of spin-coated cellulose-xyloglucan multilayered thin films. Langmuir 26 (22), 17248–17255.

Chiarelli, P.A., Johal, M.S., Holmes, D.J., Casson, J.L., Robinson, J.M., Wang, H.-L., 2002. Polyelectrolyte spin-assembly. Langmuir 18 (1), 168–173.
Cummings, J., Lowengrub, J.S., Sumpter, B.G., Wise, S.M., Kumar, R., 2018. Modelling solvent evaporation during thin film formation in phase separating polymer mixtures. Soft Matter 14 (10), 1833–1846.
De Gennes, P.G., 2001. Instabilities during the evaporation of a film: non-glassy polymer + volatile solvent, The. Eur. Phys. J. E 6, 421–424.
De Gennes, P.G., 2002. Solvent evaporation of spin cast films: "crust" effects. Eur. Phys. J. E 7 (1), 31–34.
Decher, G., 1997. Fuzzy nanoassemblies: toward layered polymeric multicomposites. Science 277, 1232–1237.
DowCellulosics, ETHOCEL, Ethylcellulose Polymers Technical Handbook, 2005.
Ebbens, S., Hodgkinson, R., Parnell, A.J., Dunbar, A., Martin, S.J., Topham, P.D., Clarke, N., Howse, J.R., 2011. In situ imaging and height reconstruction of phase separation processes in polymer blends during spin coating. ACS Nano 5 (6), 5124–5131.
Fager, C., 2018. 3D Reconstruction of Porous and Poorly Conductible Soft Materials using FIB-SEM Tomography. Physics, Eva Olsson Group, Chalmers University of Technology, Goteborg, Chalmers, p. 44.
Fager, C., 2020. Quantitative 3D Reconstruction of Porous Polymers using FIB-SEM Tomography. Chalmers University of Technology, Gothenburg, Sweden, Department of Physics, p. 74.
Fager, C., Barman, S., Röding, M., Olsson, A., Lorén, N., von Corswant, C., Bolin, D., Rootzen, H., Olsson, E., 2020a. 3D high spatial resolution visualisation and quantification of interconnectivity in polymer films. Int. J. Pharm. 587, 119622.
C. Fager, C. von Corswant, M. Röding, A. Viridén, M.-O. Johansson, A. Olsson, N. Lorén, E. Olsson, Correlating release properties with porous structure of pellet coatings used for controlled drug release. In: Manuscript (Ed.), International Journal of Pharmaceutics, 2021.
Fager, C., Röding, M., Olsson, A., Lorén, N., von Corswant, C., Sarkka, A., Olsson, E., 2020b. Optimization of FIB-SEM tomography and reconstruction for soft, porous, and poorly conducting materials. Microsc. Microanal. 26 (4), 837–845.
Fager, C., Gebäck, T., Hjärtstam, J., Röding, M., Olsson, A., Lorén, N., Von Corswant, C., Särkkä, A., Olsson, E., 2021b. Correlating 3D porous structure in polymer films with mass transport properties using FIB-SEM tomography. Chem. Eng. Sci.: X 12, 100109.
Flory, P.J., 1942. Thermodynamics of high polymer solutions. J. Chem. Phys. 10 (1), 51–61.
Gebäck, T., Marucci, M., Boissier, C., Arnehed, J., Heintz, A., 2015. Investigation of the effect of the tortuous pore structure on water diffusion through a polymer film using lattice Boltzmann simulations. J. Phys. Chem. B 119 (16), 5220–5227.
Heinrich, S., Dosta, M., Antonyuk, S., 2015. Multiscale analysis of a coating process in a Wurster fluidized bed apparatus. Mesoscale Model. Chem. Eng. Part I 83–135. https://doi.org/10.1016/bs.ache.2015.10.012.
Henderson, I.C., Clarke, N., 2004. Two-Step Phase Separation in Polymer Blends. Macromolecules 37 (5), 1952–1959.
Heriot, S.Y., Jones, R.A., 2005. An interfacial instability in a transient wetting layer leads to lateral phase separation in thin spin-cast polymer-blend films. Nat. Mater. 4 (10), 782–786.
Huang, C., Olvera de la Cruz, M., Swift, B.W., 1995. Phase separation of ternary mixtures: symmetric polymer blends. Macromolecules 28, 7996–8005.
Johnston, A.P.R., Cortez, C., Angelatos, A.S., Caruso, F., 2006. Layer-by-layer engineered capsules and their applications. Curr. Opin. Colloid Interface Sci. 11 (4), 203–209.
Kim, J.Y., Cho, C.H., Palffy-Muhoray, P., Kyu, T., 1993. Polymerization-induced phase separation in a liquid-crystal-polymer mixture. Phys. Rev. Lett. 71 (14), 2232–2235.
Kim, C.-S., Saylor, D.M., McDemott, M.K., Patardhan, D.V., Warren, J.A., 2009. Modeling solvent evaporation during the manucfacture of controlled drug-release coatings and the impact on release kinetics. J. Biomed. Mater. Res. B Appl. Biomater. 90 (2), 688–699.
Kramer, E.J., Green, P., Palmström, C.J., 1984. Interdiffusion and marker movements in concentrated polymer-polymer diffusion couples. Polymer (25) 473–480.
Marucci, M., Ragnarsson, G., von Corswant, C., Welinder, A., Jarke, A., Iselau, F., Axelsson, A., 2011. Polymer leaching from film coating: effects on the coating transport properties. Int. J. Pharm. 411 (1–2), 43–48.
Meyerhofer, D., 1978. Characteristics of resist films produced by spinning. J. Appl. Phys. 49 (49), 3993–3997.
Mokarian-Tabari, P., Geoghegan, M., Howse, J.R., Heriot, S.Y., Thompson, R.L., Jones, R. A., 2010. Quantitative evaluation of evaporation rate during spin-coating of polymer blend films: control of film structure through defined-atmosphere solvent-casting. Eur. Phys. J. E 33 (4), 283–289.
Moreira, J., Vale, A.C., Alves, N.M., 2021. Spin-coated freestanding films for biomedical applications. J. Mater. Chem. B 9 (18), 3778–3799.
Muller-Buschbaum, P., Stamm, M., 2001. Film Thickness dependence of the domain size in weakly incompatible thin polymer blend films. Colloid Polym. Sci. 279, 376–381.
Negi, V., Wodo, O., van Franeker, J.J., Janssen, R.A.J., Bobbert, P.A., 2018. Simulating phase separation during spin coating of a polymer-fullerene blend: a joint computational and experimental investigation. ACS Appl. Energy Mater. 1 (2), 725–735.
Oono, Y., Puri, S., 1987. Study of phase-separation dynamics by use of cell dynamical systems. II. Two-dimensional demonstrations. Phys. Rev. A 38, 434–453.
Raj Kumar, A., 2012. Drying induced phase separation. J. Chem. Eng. 27, 12–20.
Ren, A.R., Hamley, I.W., 2001. Cell dynamics simulations of microphase separation in block copolymers. Macromolecules 34, 116.
Röding, M., Fager, C., Olsson, A., von Corswant, C., Olsson, E., Lorén, N., 2021. Three-dimensional reconstruction of porous polymer films from FIB-SEM nanotomography data using random forests. J. Microsc. 281, 76–86.
Ronsin, O.J.J., Jang, D., Egelhaaf, H.-J., Brabec, C.J., Harting, J., 2020. A phase-field model for the evaporation of thin film mixtures. PCCP 22 (12), 6638–6652.
Sakellariou, P., Rowe, R.C., 1995. Interactions in cellulose derivative films for oral drug delivery. Prog. Polym. Sci. 20 (5), 889–942.
Saylor, D.M., Guyer, J.E., Wheeler, D., Warren, J.A., 2011. Predicting microstructure development during casting of drug-eluting coatings. Acta Biomater. 7 (2), 604–613.
Schindelin, J., Arganda-Carreras, I., Frise, E., Kaynig, V., Longair, M., Pietzsch, T., Preibisch, S., Rueden, C., Saalfeld, S., Schmid, B., Tinevez, J.-Y., White, D.J., Hartenstein, V., Eliceiri, K., Tomancak, P., Cardona, A., 2012. Fiji: an open-source platform for biological-image analysis. Nat. Methods 9 (7), 676–682.
Schmid, B., Schindelin, J., Cardona, A., Longair, M., Heisenberg, M., 2010. A high-level 3D visualization API for Java and ImageJ. BMC Bioinf. 11 (1), 274.
Tanaka, H., 1994. Double phase separation in a confined, symmetric binary mixture: Interface quench effect unique to bicontinuous phase separation. Phys. Rev. Lett. 72 (23), 3690–3693.
Tanaka, H., Araki, T., 1998. Spontaneous double phase separation induced by rapid hydrodynamic coarsening in two-dimensional fluid mixtures. Phys. Rev. Lett. 81 (2), 389–392.
Tiwari, G., Tiwari, R., Sriwastawa, B., Bhati, L., Pandey, S., Pandey, P., Bannerjee, S.K., 2012. Drug delivery systems: an updated review. Int. J. Pharm. Invest. 2 (1), 2–11.
Tran, T.L., Chan, P.K., Rousseau, D., 2006. Morphology control in symmetric polymer blends using two-step phase separation. Comput. Mater. Sci 37 (3), 328–335.
Tyona, M.D., 2013. A theoritical study on spin coating technique. Adv. Mater. Res. 2 (4), 195–208.
van Franeker, J.J., Westhoff, D., Turbiez, M., Wienk, M.M., Schmidt, V., Janssen, R.A.J., 2015. Controlling the dominant length scale of liquid-liquid phase separation in spin-coated organic semiconductor films. Adv. Funct. Mater. 25 (6), 855–863.
S. Wassén, R. Bordes, T. Gebäck, D. Bernin, E. Schuster, N. Lorén, A.-M. Hermansson, Probe diffusion in phase-separated bicontinuous biopolymer gels (2014). https://doi.org/10.1039/C4SM01513D.
Williams, E.L., Gorelik, S., Phang, I., Bosman, M., Vijila, C., Subramanian, G.S., Sonar, P., Hobley, J., Singh, S.P., Matsuzaki, H., Furube, A., Katoh, R., 2013. Nanoscale phase domain structure and associated device performance of organic solar cells based on a diketopyrrolopyrrole polymer. RSC Adv. 3 (43), 20113.
Yamamura, M., Nishio, T., Toshihisa, K., Atachi, K., 2002. Evaporation-induced pattern formation in polymer films via secondary phase separation. Chem. Eng. Sci. 57, 2901–2905.